TRIBHUVAN UNIVERSITY

INSTITUTE OF ENGINEERING

PULCHOWK CAMPUS

A THESIS REPORT ON

GREEN SYNTHESIS OF CARBON QUANTUM DOTS FROM BANANA PEELS AND THEIR APPLICATION IN HEAVY METAL (FE^{3+}) SENSING

SUBMITTED BY:

AYUSHA KAFLE

(080MSMSE003)

SUPERVISED BY:

PROF. DR. KHEM RAJ SHRESTHA

SUBMITTED TO:

DEPARTMENT OF APPLIED SCIENCE & CHEMICAL ENGINEERING

May, 2026

Declaration

I hereby declare that this study/research entitled **GREEN SYNTHESIS OF CARBON QUANTUM DOTS FROM BANANA PEELS AND THEIR APPLICATION IN HEAVY METAL Fe^{3+} SENSING** is based on our original research work. Related works on the topic by other researchers have been duly acknowledged. I owe all the liabilities relating to the accuracy and authenticity of the data and any other information included hereunder.

Ayusha Kafle (080MSMSE003)

Date: 2026/05/1

Recommendation

This is to certify that this project report entitled **GREEN SYNTHESIS OF CARBON QUANTUM DOTS FROM BANANA PEELS AND THEIR APPLICATION IN HEAVY METAL Fe^{3+} SENSING**] prepared and submitted by **Ayusha Kafle (080MSMSE003)**, in partial fulfillment of the requirements of the Master degree of Engineering in Material Science awarded by Tribhuvan University, has been completed under my supervision. I recommend the same for acceptance by Tribhuvan University.

Name of the Supervisor: Dr. Khem Raj Shrestha
Designation: Professor
Organization: Pulchowk Campus, Ioe
Date: 2026/05/01

Page of Approval

TRIBHUVAN UNIVERSIY
INSTITUTE OF ENGINEERING
PULCHOWK CAMPUS
DEPARTMENT OF ELECTRONICS AND COMPUTER ENGINEERING

This project/thesis entitled **GREEN SYNTHESIS OF CARBON QUANTUM DOTS FROM BANANA PEELS AND THEIR APPLICATION IN HEAVY METAL Fe^{3+} SENSING** prepared and submitted by **Ayusha Kafle (080MSMSE003)** has been examined by us and is accepted for the award of the Master's degree in Material Science and Engineering by Tribhuvan University.

.....	.....
Supervisor	External examiner
Khem Raj Shrestha	**Name**
Professor	Designation
Pulchowk Campus, Kathmandu, Nepal.	Organization Name and Address.

Date of approval: 2026/05/01

Copyright

Acknowledgments

I would like to express my deepest gratitude to the Department of Applied Science and Chemical Engineering, Pulchowk Campus,Tribhuvan University, Nepal for providing all the necessary laboratory and resources. am especially grateful to my supervisor,Dr.Khemraj Shrestha for his valuable guidance and advice throughout the project. I would also like to acknowledge ASCOL Campus for granting access to the PerkinElmer FTIR spectrometer used in this study. Their support in facilitating instrumental analysis is highly appreciated.

Finally, I extend my heartfelt thanks to my friends and family for their constant encouragement, understanding, and support during the completion of this work.

Ayusha Kafle (080MSMSE003)

Abstract

Carbon quantum dots (CQDs) are the materials of the carbon family that has a size less than 10 nm and it has gained enormous attention from the researchers worldwide since the last decade due to their tunable properties like water solubility, low toxicity, and excellent photoluminescence and multiple technical application. In this research, Carbon quantum dots were successfully synthesized via a facile hydrothermal method using banana peel as a sustainable carbon precursor at a mild synthesis temperature of 130°C for 12 hours. The synthesized CQDs were characterized using UV-Vis spectrophotometry, UV chamber fluorescence analysis, and Fourier Transform Infrared (FTIR) spectroscopy, which confirmed characteristic absorption peaks at 270 nm ($\pi \rightarrow \pi^*$ transitions) and 285.5 ($n \rightarrow \pi^*$ transitions), as well as vivid blue-green photoluminescence under 365 nm UV excitation. The CQDs demonstrated selective sensing capability toward Fe^{3+} ions, with UV-Vis absorbance decreasing progressively from 1.041 a.u. (0 μM) to 0.710 a.u. (150 μM), corresponding to fluorescence quenching efficiencies of 5%, 22.8%, and 31.8% at Fe^{3+} concentrations of 50,100 and 150 μM respectively. The concentration dependent quenching behavior confirms the potential of banana peel derived CQDs as a cost-effective,eco-friendly sensing platform for Fe^{3+} detection.

Keywords: *Fluorescence quenching, Carbon Quantum dots, Green synthesis, Nonmaterial,Optical sensing*

Contents

Declaration ii

Recommendation iii

Page of Approval iv

Copyright v

Acknowledgements vi

Abstract vii

Contents x

List of Figures xi

List of Tables xii

List of Abbreviations xiii

List of Units and conversions xiv

1 Introduction 1

1.1 Background 1

1.2 Statement of the Problem 3

1.3 Research objectives 3

1.3.1 General Objective 3

1.3.2 Specific Objectives 4

1.4 Rationale of the Study 4

1.5 Scope and Limitation of the study 5

2 Literature Review 6

2.1 Introduction to Carbon Quantum Dots (CQDs) 6

2.2 Classification of Carbon Based Fluorescent Nanomaterials 6

2.3 Optical and Electronic Properties 7

2.4 Synthesis Methods for Carbon Quantum Dots 8
2.4.1 Top-Down Approaches 8
2.4.2 Bottom-Up Approaches 8
2.4.3 Pyrolysis and Carbonization 9
2.5 Green Synthesis of CQDs from Biomass 10
2.5.1 Rationale for Green Synthesis 10
2.5.2 Banana Peel as a Precursor for CQD Synthesis 10
2.5.3 Other Biomass Derived CQDs: Comparative Overview 11
2.6 Photoluminescence Mechanisms in Carbon Quantum Dots 11
2.6.1 Proposed Mechanisms of Fluorescence 11
2.6.2 Excitation Dependent Emission and Red-Shifting 11
2.6.3 Role of Surface Functional Groups 11
2.7 Structural Characterization of CQDs 12
2.7.1 Morphological Characterization 12
2.7.2 Crystallographic Characterization 12
2.7.3 Spectroscopic Characterization 13
2.8 Applications of CQDs in Heavy Metal Ion Sensing 13
2.8.1 Principles of Fluorescent Sensing 13
2.8.2 Detection of Fe^{3+} Ions 13
2.8.3 Detection of Other Heavy Metal Ions 14
2.9 Biocompatibility and Other Applications of CQDs 14
2.10 Research Gaps and Justification for the Present Study 14

3 Experimental **16**
3.1 Materials 16
3.2 Methodology 16
3.2.1 Raw Material Preparation 16
3.2.2 Synthesis of Carbon Quantum Dots by Hydrothermal Method 18
3.3 Purification and Characterization of Carbon Quantum Dots 20
3.3.1 Preparation of Fe^{3+} Stock Solution 21
3.4 Preparation of CQD–Fe^{3+} Samples for Fluorescence Sensing 22
3.4.1 UV–Vis Spectrophotometric Analysis 23
3.4.2 FTIR Spectroscopy 24

4 Result and Discussion **26**
4.1 Material Synthesis 26
4.2 Mechanism of Hydrothermal Synthesis 26

4.2.1 Electron Transfer Mechanism of Fe^{3+} Sensing 27
4.3 Characterization 28
4.3.1 UV Chamber Fluorescence Analysis 29
4.3.2 UV-Vis Spectrophotometric Characterization 32
4.3.3 FTIR Characterization 35
4.4 Application: Fe^{3+} Sensing 36
4.4.1 Summary of Spectral Parameters 37
4.4.2 Individual Absorption Spectra 38
4.5 Conclusion 41

5 Limitations and Future enhancement **42**
5.1 Limitations 42
5.2 Future Enhancements 42
References 43

List of Figures

3.1 Diagrammatic representation of the preparation of raw material. 18
3.2 Diagrammatic representation of hydrothermal synthesis. 20

4.1 Carbon quantum dots under normal daylight, 365nm uv light and 254 nm uv light respectively. 30
4.2 Carbon quantum dots solution under uv lamp. 30
4.3 Ethanol diluted Carbon quantum dots solution under uva lamp. 31
4.4 Distilled water diluted Carbon quantum dots solution under uva lamp. . . . 31
4.5 Photographs of CQD solutions with 0, 50, 100, and 150 μM Fe^{3+} under short-wave UV irradiation (254 nm). 31
4.6 Absorbance VS Wavelength of sample diluted with ethanol. 33
4.7 Absorbance VS Wavelength of sample diluted with distilled water. 34
4.8 Absorbance VS Wavelength of Undiluted CQDs. 34
4.9 FTIR spectrum of CQDs synthesized from banana peel. 36
4.10 UV-Vis absorbance spectrum of CQDs only (0 μM Fe^{3+}) 38
4.11 UV-Vis absorbance spectrum of CQDs + 50 μM Fe^{3+} 39
4.12 UV-Vis absorbance spectrum of CQDs + 100 μM Fe^{3+} 40
4.13 UV-Vis absorbance spectrum of CQDs + 150 μM Fe^{3+} 40

List of Tables

4.1 Summary of UV-Vis spectral parameters at each Fe^3+concentration 38

List of Abbreviations

QDs	Quantum Dots
CQDs	Carbon Quantum Dots
UV	Ultraviolet
UV-Vis	Ultraviolet Visualization

List of units and conversions

°C	Degree Celsius
L	Liter
g	gram
mL	mililiter
μM	Micromolar
nm	Nanometer

1. Introduction

1.1 Background

Rapid urbanization and industrialization has led to worldwide environmental pollution. This increase in pollution is caused by the combination of issues like increase in organic waste from agricultural activities and the simultaneous increase in heavy metal pollution in water resources. Nepal's agricultural sector produces huge amounts of waste biomass after harvest each year [1]. Post-harvest losses of fruits and vegetables are estimated to range from 20–50%, which is caused mainly by lack of cold storage facilities and poor packaging leading to significant organic waste generation [1]. During the study of major wholesale market in many places of Nepal like Kalimati,Pokhara, and Narayangadh it was confirmed that kalimati market generates upto 20 tons of vegetable waste daily during peak production months [1]. These wastes including fruit peels, seeds, and Pulp residues, are often discarded without utilizing it properly which only contributes to further environmental pollution [2]. In recent years, there has been significant interest in turning low value biomass waste into value added nano material [3]. These biomass wastes are particularly rich in carbon compounds like carbohydrates, cellulose, and lignin making them suitable as precursors for synthesis of carbon-based nanomaterials [4]. Among such nanomaterials, carbon quantum dots (CQDs) have recently gained attention as highly versatile fluorescent nanoparticles, used in areas like sensing, optoelectronics, and bioimaging [5].

Carbon quantum dots are zero-dimensional carbon nanoparticles typically less than 10 nm in size that were accidentally discovered by Xu et al. in 2004 during the electrophoretic purification of single-walled carbon nanotubes [6]. Later, Sun et al. in 2006 introduced the term 'carbon quantum dots' and demonstrated improved photoluminescence by using laser ablation on carbon based precursors[7]. Carbon quantum dots possess unique properties like water solubility, high chemical stability, low toxicity which have attracted significant interest of researchers for the applications like optoelectronic devices, biomedical labeling and electrochemical sensors [8]. The properties of carbon quantum dots stand in sharp contrast to conventional semiconductor quantum dots that contain toxic heavy metals [9].

There are various synthesis techniques for the preparation of CQDs,broadly categorized into top-down and bottom-up approaches [10]. Top-down methods include laser ablation, arc discharge, and electrochemical oxidation, which involve breaking down large carbon structures into nanoscale particles, but are generally energy intensive and expensive[7]. Bottom-

up approaches such as hydrothermal synthesis, microwave- assisted synthesis, and pyrolysis build CQDs from small molecular precursors and are generally simpler and more eco-friendly [11]. For the synthesis of CQDs, the hydrothermal synthesis is mostly preferred as it can operate at moderate temperatures, requires no hazardous solvents, and produces CQds with rich surface functional groups essential for sensing applications[12].

Green synthesized CQDs from fruit and vegetable biomass have attracted particular attention because they are more cost-effective, stable, and require less energy than conventional methods[13]. Banana peel, a common agricultural waste is a particularly promising material due to its high levels of carbohydrates and cellulose content, which provide carbon rich cores for CQD formation,as well as nitrogen containing functional groups that enhance quantum yeild [14]. Previous researches have shown that CQDs synthesized from banana peels exhibit strong blue fluorescence, good photostability and excellent water dispersibility without using extra surface passivation chemicals[15].

Meanwhile, contamination of water sources with heavy metals has emerged as an urgent environmental and public health crisis[16]. Manufacturing, mining, industrial production, and agriculture have introduced significant amounts of heavy metals into the soil, water and atmosphere causing toxic risks to ecosystem [17]. Heavy metals alters the physical and chemical properties of the soil, impacting both plants and animals[17]. Iron (Fe^{3+}) is one of the most prevalent metal ions found in industrial effluents,groundwater and surface water system [18]. While iron is an essential trace element for biological functions including oxygen transport and enzyme activity, its excessive presence in the aquatic systems can cause severe ecological imbalance through oxidative stress and alteration of the physiochemical properties of water. [19] . Conventional analytical techniques for heavy metal detection such as atomic absorption spectroscopy and inductively coupled plasma mass spectrometry (ICP-MS) provide high accuracy and sensitivity [20]. However, these techniques require expensive instruments, trained personnel, and complex sample preparation procedures, limiting their application in resource- constrained settings such as Nepal [21]. There is therefore a growing demand for simple,cost effective, and portable sensing platforms capable of detecting Fe^{3+} at low concentrations. CQD based fluorescent sensors have gained attention as strong candidates to meet the demand [22]. The fluorescence of CQDs can be specifically reduced by Fe^{3+} ions through mechanisms like inner filter effect, static quenching, and electron or energy transfer interactions between Fe^{3+} and functional groups on the CQD surface such as hydroxyl, carboxyl, and amino groups [21].

Although there has been significant progess worldwide in this ares, studies on producing CQDs from fruit waste in Nepal and its application to local environmental monitoring are still vastly unexplored. With Nepal generating large amounts of fruit waste biomass and the

urgent demand for affordable heavy metal sensing, there is a strong scientific and socioeconomic rationale to develop banana peel derived CQDs as fluorescent probes for detecting Fe^{3+}.

1.2 Statement of the Problem

Nepal is dealing with a interconnected set of environmental and public health problems that are both scientifically interconnected and also not addressed significantly. The first major problem is the large scale production of agricultural biomass waste, particularly fruit peel which often builds up in wholesale markets and processing areas without systematic recovery[1]. Fruit and vegetable post harvest losses of 20 % to 50 % shows that Nepal's major markets generate thousands of tons of organic waste each year [1]. Most of this waste is dumped in open dumpsites, where it contributes to greenhouse gas emission, soil pollution causing a serious and growing environmental burden[1]. The second challenge is the widespread contamination of Nepal's water bodies with heavy metal ions from both industrial and agricultural sources. Brick kilns, mining activities, and pharmaceutical manufacturing release effluents containing heavy metals into rivers and groundwater system [16]. Fe^{3+} is one of the most frequently detected contaminants which is concerning because high iron level reduce water quality and create oxidative, toxic conditions for aquatic organisms[18].The third issue is the lack of analytical methods that are fast, economical, and suitable for field use in Nepal. Standard laboratory techniques such as ICP-MS and AAS require specialized infrastructure, imported reagents, trained personnel, and relatively high operating costs which makes them difficult for most environmental monitoring agencies in the country to access. As a result contamination often go undetected until significant ecological damage has already occurred Synthesizing CQDs from locally available banana peel waste through low cost hydrothemal method offers a way to address all three issues at once. First agricultural waste is converted into value added products, producing a high value functional nanomaterial and a sensing platform is created for sensing Fe^{3+}. However, the Optical response of banana peel derived CQDs when exposed to Fe^{3+} ions has not been systematically studied using locally sourced materials. This lack of research creates a major knowledge gap that limits both scientific insight and the practical use of green CQD based sensors for environment monitoring in Nepal.

1.3 Research objectives

1.3.1 General Objective

The general objective of this research is to synthesize carbon quantum dots from banana peel waste using the hydrothermal method and to investigate their optical response to varying

concentrations of Fe^{3+} ions.

1.3.2 Specific Objectives

- To synthesize carbon quantum dots from banana peel powder using hydrothermal synthesis method at 130 °C.
- To characterize the synthesized CQDs using UV-Vis spectrophotometer to determine optical absorption properties, UV chamber observation to confirm photoluminescence and FTIR spectroscopy to identify surface functional groups.
- To study the effect of Fe^{3+} ions at concentrations of 50 μM 100 μM and 150 μM on the UV Vis absorbance behavior of CQDs.

1.4 Rationale of the Study

This research carries significant implications in terms of its scientific, environmental, and socioeconomic value in the case of Nepal, where development needs are coupled with environmental challenges. It is hence scientifically justifiable to conduct this research not only to solve the pressing issues relating to waste management but also advance science in developing green nanomaterials. Regarding the issue of waste valorization, this study contributes to the recycling of biomass wastes as useful materials. In Nepal, the fruit and vegetable wholesale markets produce high amounts of biomass in the form of peel wastes which do not have any definite means of recovery at present. This research shows that the banana peel waste can be used effectively as the starting material for synthesizing the CQDs nanomaterials. Hence, it establishes the feasibility of adopting a circular economy in handling biomass wastes in Nepal through scientific research. The study is further justified by its contribution to knowledge in the field of nanotechnology and materials science, particularly regarding green synthesized CQDs derived from fruit waste. The characterization of banana peel derived CQDs using UV–Vis spectrophotometry and FTIR spectroscopy strengthens understanding of how biomass composition can influence CQD surface chemistry and fluorescence related optical behavior. It is hoped that these results will help further refine conditions for CQD preparation by showing that various kinds of biomasses can provide CQDs that differ in their physico-chemical properties and optical properties. On the whole, the significance of the study comes from both practical and scientific perspectives. Practically, it provides a method to convert agricultural biomass waste to valuable nanomaterials. Scientifically, it adds to an already existing but small literature concerning the production of CQDs using agricultural waste biomass, which also includes biomass wastes found in Nepal.

Therefore, results obtained in this research would be of help to other researchers in similar studies.

1.5 Scope and Limitation of the study

The current study is particularly concerned with the fabrication of carbon quantum dots (CQDs) using a hydrothermal approach based on banana peels. The study also analyzes the effect of Fe^{3+} ions on the optical characteristics of the prepared CQDs. In terms of analysis, the current study utilizes UV–Vis spectrophotometry, UV chamber, and FTIR spectroscopy. The Fe^{3+} sensing is limited to three different Fe^{3+} concentration levels 50 μM, 100 μM, and 150 μM tested in aqueous solution under controlled laboratory conditions. Nonetheless, this study does not apply any structural analysis techniques such as transmission electron microscope (TEM), X-ray diffraction (XRD), and X-ray photoelectron spectroscopy (XPS). Structural analysis will reveal the size of particles, crystal structure, and chemical composition of quantum dots. Furthermore, no tests will be conducted on the selectivity and sensitivity of the sensor due to possible interferences from metal ions such as copper (Cu^{2+}), lead (Pb^{2+}), and mercury (Hg^{2+}). The measurement of the detection limit as well as Stern-Volmer quenching will be conducted using the method of fluorescence spectroscopy that is not within the scope of this study. Last but not least, this study will only make use of a single type of biomass material (banana peels) and not consider the outcomes of making quantum dots using other fruits or agricultural waste products.

2. Literature Review

2.1 Introduction to Carbon Quantum Dots (CQDs)

Carbon quantum dots (CQDs) are a relatively new type of carbon-based, zero-dimensional nanomaterials, usually with sizes smaller than 10 nm. Since their accidental discovery in 2004 during the purification of single-walled carbon nanotubes by Xu and co-workers, CQDs have gained major attention from researchers. This is largely because they exhibit distinctive and adjustable photoluminescence, along with strong biocompatibility, low cytotoxicity, good water solubility, and the ability to be easily modified through surface functionalization [6].

Unlike traditional semiconductor quantum dots that require toxic heavy metals like cadmium and lead, CQDs offer a better solution in terms of sustainability and eco-friendliness. Therefore, there are numerous applications for CQDs in different areas ranging from solar cell technology, biomedical imaging, photocatalysis, photonic devices, and chemical sensors.

Carbon quantum dots are fluorescent carbon based nanoparticles that were first reported by Sun and co-workers in 2006 after surface passivation of carbon nanoparticles produced by arc discharge. In their work, Sun et al. showed that CQDs can emit strong photoluminescence in both liquid solution and the solid state, even with simple surface passivation. This study helped establish the key optical behavior of CQDs and highlighted their promise for sensing and imaging applications [7]. Overall, this early research marked an important turning point in nanomaterials, providing a non-toxic, widely available carbon-based alternative to traditional semiconductor quantum dots.

Before the term "carbon quantum dots" became commonly used, related fluorescent carbon nanomaterials were often referred to by different names, such as carbon nanodots, carbon dots (C-dots), and graphene quantum dots (GQDs). Although these materials share many similar characteristics, they differ in their internal structure and the extent of graphitization, which is discussed in the section below.

2.2 Classification of Carbon Based Fluorescent Nanomaterials

The broader family of fluorescent carbon nanomaterials can be divided into three main subgroups: carbon quantum dots (CQDs), graphene quantum dots (GQDs), and carbon nanodots (CNDs). CQDs are generally quasi-spherical particles that are amorphous or

semi-crystalline and are commonly functionalized with oxygen-containing groups on their surface. GQDs, on the other hand, are made from single- or few-layer graphene sheets with lateral sizes typically below 10 nm, where their two-dimensional structure leads to quantum confinement effects. Carbon nanodots are amorphous carbon particles that do not have a crystalline graphene core. In this study, the main focus is on CQDs which are usually described as having an sp^2 hybridized carbon core, with contributions from sp^3 carbon, along with a large number of surface functional groups such as hydroxyl (–OH), carboxyl (–COOH), carbonyl ($–C = O$), and amino ($–NH^2$) groups. These surface moieties are essential because they strongly influence both the photoluminescent behavior and the chemical sensing performance of the nanoparticles.

2.3 Optical and Electronic Properties

One of the most impressive and widely useful features of CQDs is their strong photoluminescence that depends on the excitation wavelength. Unlike conventional organic dyes, which usually emit at a fixed wavelength, CQDs show a noticeable shift in their emission peak when the excitation wavelength changes. This effect is generally linked to the CQDs' size distribution as well as the presence of different surface states created by a variety of functional groups[7]. As a result, CQDs can be used for multicolor imaging and for multiplexed sensing, using essentially the same nanomaterial system.

The UV-Vis absorption spectra of CQDs commonly show distinct absorption features in the 250–400 nm region. An absorption peak around 280–290 nm is usually linked to $\pi \rightarrow \pi^*$ electronic transitions associated with aromatic $C = C$ bonds in the sp^2 conjugated carbon core. In addition, a shoulder or a band near 320–340 nm is often attributed to $n \rightarrow \pi^*$ transitions coming from surface carbonyl $C = O$ groups [23]. These match the report by Lee and Ko (2025), who observed characteristic peaks at 289 nm (related to $C = C$ bonds) and around 330 nm for CQDs synthesized from pulp using hydrothermal processing results that are also consistent with what is seen in the present study. The concept of quantum yield (QY) plays an important role in determining the fluorescence efficiency of materials. Quantum yield is defined as the ratio of emission to absorption photons. CQDs prepared by various methods show a large difference in their quantum yields. The value of QY of CQDs varies from 5% to 80%, depending on several factors, including carbon sources, methods of preparation, and surface passivation. For example, Kumari et al. [23] reported that the microwave-assisted pyrolysis of CQDs at 500 W and 5 minutes showed a QY of about 14%. This result can be compared with results obtained from research on CQDs synthesized by the hydrothermal method.

2.4 Synthesis Methods for Carbon Quantum Dots

Various different methods have been developed for synthesizing CQDs, which can be classified into bottom-up and top-down methodologies. The unique advantages offered by each method include control over particle size, surface chemistry, scalability, and environmental impact.

2.4.1 Top-Down Approaches

Top-down techniques entail the mechanical and/or chemical disassembly of larger molecules of carbon-based nature into smaller nanometer-sized structures. Some of the frequently employed top-down techniques are arc discharge, laser ablation, electrochemical oxidation, and chemical oxidation. One of the first methods described for the preparation of CQDs was the arc-discharge technique; but in general, these techniques are highly energy-consuming, need expensive equipment, and lack the capability to control the particle size and chemistry. The electrochemical methods, although controllable, are less scalable and do not easily lend themselves to functionalization with biochemically important groups.

2.4.2 Bottom-Up Approaches

In bottom-up synthesis, the formation of CQDs occurs via chemical reactions between molecular precursors. This method provides better control over the size of the particles, surface chemistry, and optical properties. Some examples of the bottom-up process include hydrothermal/solvothermal synthesis, microwave-assisted synthesis, pyrolysis, and combustion.

Hydrothermal Synthesis

By far, hydrothermal synthesis has been the most prevalent bottom-up approach to synthesizing CQDs from biological precursors. Herein, a solution or suspension of the carbon-containing compound is placed in a closed vessel known as an autoclave, which is then heated to high temperatures (120-250°C). Heating causes the autoclave's pressure to rise significantly, thereby increasing the boiling point of water beyond its normal level. As a result, chemical processes take place that otherwise would have been impossible at atmospheric pressure to produce CQDs. The hydrothermal route is especially promising in terms of environmentally friendly approaches due to its simplicity, which involves the use of only water as the medium, acceptance of various bio-based feedstocks, and production of CQDs using a one-step process without the utilization of any hazardous reagents. Prasannan and Imae successfully developed an innovative one-pot hydrothermal synthesis technique for the formation of fluorescent CQDs using orange peels as raw material, with the entire synthesis process being performed at a relatively low temperature of 180°C [24]. This work established

orange peel and by extension, other citrus and fruit byproducts as viable green precursors for CQD synthesis. Atchudan et al. (2021) synthesized CQDs from banana peel waste by hydrothermal treatment at 200 °C for 24 hours, obtaining nanoparticles with a narrow particle size distribution averaging 5 nm and demonstrating strong photoluminescence suitable for in vivo bioimaging applications [12]. Similarly, Parambil et al. (2024) performed a systematic one-step hydrothermal synthesis of highly fluorescent CQDs from different varieties of banana peels, wherein dried peel powder was mixed with distilled water and heated at 180 degrees C for 12 hours, yielding CQDs with selective sensing capability for Fe^{3+} ions [5]. More recently, Lee and Ko (2025) explored the effect of synthesis parameters temperature, reaction time, and pulp consistency on the properties of hydrothermally synthesized CQDs, demonstrating that particle emission peaks red-shift at longer excitation wavelengths [25]. Purwamargapratala et al. (2024) synthesized CQDs from Musa paradisiaca (banana) peels by the hydrothermal method, with XRD analysis confirming the amorphous carbon structure characteristic of CQDs, and demonstrated their potential as an additive in lithium-ion batteries[26].

Microwave Assisted Synthesis

Microwave-assisted synthesis has emerged as a rapid and energy efficient alternative to hydrothermal synthesis. In this approach, microwave irradiation provides rapid volumetric heating of the precursor solution, enabling the formation of CQDs in a matter of minutes rather than hours. Kumari et al. (2022) demonstrated microwave pyrolysis at 500 W for 5 minutes as an effective route to fluorescent CQDs from bio-derived precursors, achieving a quantum yield of approximately 14% [23]. Alansari et al. (2025) also adopted a one-step microwave-assisted method to synthesize CQDs functioning as efficient fluorescent chemosensors for Hg^{2+} and Fe^{3+}detection, further validating the applicability of microwave synthesized green CQDs for heavy metal sensing [13]. Despite its advantages in decreasing reaction times, microwave synthesis tends to be less accurate in controlling particle sizes than hydrothermal synthesis, and may not be applicable to large-scale synthesis.

2.4.3 Pyrolysis and Carbonization

Pyrolysis involves the thermal decomposition of organic precursors at elevated temperatures in the absence of oxygen. Pandiyan et al. (2020) reported a two-step approach in which sun-dried sugarcane bagasse pulp was first heated at 60 degrees C to form a carbon matrix, which was then mixed with citric acid and treated in a hydrothermal autoclave at 200 degrees C for 6 hours, yielding biocompatible CQDs with effective nonlinear optical behavior and antimicrobial activity [27]. This work showed that combining pyrolysis with hydrothermal

processing can enhance the properties of the resulting CQDs.

2.5 Green Synthesis of CQDs from Biomass

2.5.1 Rationale for Green Synthesis

Efficient and economic synthesis strategies that are environmentally friendly have been extensively researched by scientists within the last decade. Compared to conventional techniques that use man-made organic compounds, green chemistry strategies that use biodegradable biomass, agricultural and food industry wastes as sources of carbon atoms can provide several advantages. Some of the advantages include using easily accessible and cheap raw materials, eliminating hazardous solvents and chemicals, and adhering to the principles of green chemistry and circular economy. Moreover, the inherent surface modification of CQDs due to various organic compounds within natural biomass contributes to enhanced luminescence efficiency without the need for further surface passivation treatments. The wide variety of carbon precursors from biomass, along with the processes involved in making fluorescent CQDs, was extensively covered by Kumari et al. (2022) [23]. CQDs from biomass can be created using a huge number of precursors that include fruit peel (such as citrus, banana, and mango); agriculture waste (such as sugarcane bagasse, rice husk, and corn cob); coffee grounds; tea leaves; plant extracts; and microorganisms.

2.5.2 Banana Peel as a Precursor for CQD Synthesis

The different types of biomass sources available include the use of banana peels as a source for CQDs because of the global availability, lack of any commercial value as waste, and higher amounts of cellulose, hemicellulose, lignin, and pectin present. The latter is a type of polymer composed of carbon and oxygen and forms fluorescent CQDs when hydrothermally treated. One of the first teams to explore CQDs extracted from banana peels was Atchudan et al. in 2021. They were able to extract CQDs with a size range of 5 nm and intense blue photoluminescence, which could be used for in vivo bioimaging applications [12]. Parambil et al. furthered this work by studying the correlation between different types of banana peels, CQD properties, and Fe^{3+} ion sensing capability under 180°C hydrothermal conditions for 12 hours [5]. The amorphous nature of banana peel CQDs was confirmed by Purwamargapratala et al. in 2024 through XRD analysis and potential energy storage applications were investigated.[26]. The present study builds upon this body of evidence by investigating the hydrothermal synthesis of CQDs from banana peel at the notably low temperature of 130 degrees C — substantially lower than the 180-200 degrees C employed in most prior studies — contributing toward more energy-efficient green synthesis approaches while retaining the desirable optical and sensing properties of the resulting CQDs.

2.5.3 Other Biomass Derived CQDs: Comparative Overview

In addition to the banana peel, there have been many other sources of fruits and agricultural waste used as precursors for CQD production. According to Prasannan and Imae (2013), orange peel waste can serve as a good precursor when synthesizing CQDs using hydrothermal method at a temperature of 180 degrees Celsius, resulting in CQDs with proven nanometer size and photoluminescence[24]. Pandiyan et al. (2020) used sugarcane bagasse pulp, which is one of the largest industrial waste materials, as a precursor for generating biocompatible CQDs that showed antimicrobial properties and nonlinear optics

2.6 Photoluminescence Mechanisms in Carbon Quantum Dots

2.6.1 Proposed Mechanisms of Fluorescence

Despite extensive research, the exact photoluminescence (PL) mechanism in CQDs remains a subject of active debate and is likely multifactorial.A number of mechanisms have been suggested to explain the phenomenon of PL in CQDs, which include: (i) quantum confinement effects that occur due to the finite size of the carbon core; (ii) emission resulting from surface states due to the diversity of functional groups on the particle surface; (iii) molecular fluorescence from individual molecules or fluorophores created during the formation process; and (iv) energy trapping at defect sites in the carbon material. The mechanism responsible for the excitation-dependent PL characteristics in CQDs, which are common to most CQDs, is primarily associated with the non-uniformity in the size of particles and surface states in the particular CQD solution. The smaller-sized particles with significant quantum confinement effects exhibit lower PL emission peaks (blue emission), while the larger-sized particles with more surface functional groups exhibit higher PL emission peaks (yellow emission).

2.6.2 Excitation Dependent Emission and Red-Shifting

According to Lee and Ko (2025), CQDs made from pulp through the use of hydrothermal technique have shown blue-green fluorescence under the excitation of 370 nm, with the peak being red shifted as the excitation wavelength increases [25]. The aforementioned observation is due to the polydispersed nature of CQDs that have been synthesized hydrothermally, which is a common attribute among CQDs obtained from biomass.

2.6.3 Role of Surface Functional Groups

The surface functional groups of CQDs that mainly consist of hydroxyl groups, carboxyl groups, carbonyl groups, and amino groups act as a dual factor influencing the optical be-

havior of CQDs and their chemical sensing ability. As first reported by Sun et al., surface passivation can lead to increased PL intensity through elimination of non-radiative recombination processes occurring on the surface of the nanoparticle [7]. The inherent passivation provided by CQDs produced from biomass owing to the presence of oxygenated functional groups formed from cellulose, hemicellulose, and lignin decomposition products accounts for the high PL quantum yield. The analysis of surface functional groups present on the surface of CQDs can be carried out using Fourier transform infrared (FTIR) spectroscopy. The typical FTIR peaks associated with different bonds include the broad $O--H$ stretch vibration peak appearing at 3200-3500 cm^{-1}, the $C--H$ stretch vibration peak appearing at 2900 cm^{-1}, the $C=O$ stretch vibration of carboxyl groups appearing at 1700 cm^{-1}, the $C=C$ stretch vibration of aromatic rings appearing at 1600 cm^{-1}, and $C--O$ stretch vibration at 1000-1200 cm^{-1}.

2.7 Structural Characterization of CQDs

2.7.1 Morphological Characterization

Transmission electron microscopy (TEM) is the primary technique for characterizing the size, morphology, and internal structure of CQDs. TEM images typically reveal quasi-spherical nanoparticles with narrow size distributions in the range of 2 to 10 nm for hydrothermally synthesized CQDs. Prasannan and Imae (2013) confirmed the nanoscale dimensions of orange peel-derived CQDs by TEM [24], while Atchudan et al. (2021) reported an average size of 5 nm with a narrow particle size distribution for banana peel CQDs[12]. High-resolution TEM (HRTEM) can further reveal lattice fringes indicative of graphitic crystalline domains within the CQD core, with d-spacings typically around 0.21 nm corresponding to the (100) plane of graphite.

2.7.2 Crystallographic Characterization

X-ray diffraction (XRD) is employed to assess the crystalline structure of CQDs. Most biomass derived CQDs exhibit a broad diffraction peak centered around 2 THETA = 20-25 degrees, corresponding to the (002) reflection of graphitic carbon and indicative of an amorphous or semi-crystalline carbon structure with short-range graphitic ordering. Purwamargapratala et al. (2024) confirmed that banana peel-derived CQDs possess an amorphous carbon structure by XRD analysis [26]. The broad and diffuse nature of the XRD peaks reflects the small crystallite size and structural disorder characteristic of CQDs synthesized at moderate hydrothermal temperatures.

2.7.3 Spectroscopic Characterization

UV-Vis absorption spectroscopy, photoluminescence spectroscopy, and FTIR spectroscopy are commonly used to characterize CQDs. UV-Vis spectra typically show absorption features near 280–290 nm, which are related to π-π^* transitions of C = C bonds, and a band near 320–340 nm that is associated with n-π^* transitions of C = O groups. These absorption characteristics have been reported for many hydrothermally synthesized biomass-derived CQDs[25].

Raman spectroscopy is also used to estimate the degree of graphitization and the extent of structural defects in the carbon framework. In Raman spectra, the ratio of the D band (around ~ 1350 cm^{-1}, related to disorder) to the G band (around ~ 1580 cm^{-1}, related to graphitic carbon) provides information about defects within the carbon core. CQDs with a higher D/G ratio are generally more amorphous and contain a larger number of defect sites.

2.8 Applications of CQDs in Heavy Metal Ion Sensing

2.8.1 Principles of Fluorescent Sensing

Fluorescent sensing using CQDs is based on the fact that interaction between a target analyte and the CQD surface leads to a detectable change in photoluminescence. Depending on the nature of the interaction, this change may appear as fluorescence quenching (turn-off behavior) or fluorescence enhancement (turn-on behavior). The selectivity and sensitivity of CQD-based sensors largely depend on the surface chemistry of the nanoparticles, since it determines how strongly specific analytes can interact with functional groups on the CQD surface.

2.8.2 Detection of Fe^{3+} Ions

Among heavy metal ions that have been studied with CQD-based fluorescent sensors, Fe^{3+} has attracted particular interest. Iron is an essential trace element involved in hemoglobin formation, enzymatic processes, and electron transport. However, excessive iron in biological systems and in drinking water can contribute to oxidative stress, liver-related problems, and other metabolic disorders. For this reason, detecting Fe^{3+} accurately at trace levels is important for clinical analysis, environmental monitoring, and food-related safety assessments.

CQDs are effective for Fe^{3+} sensing because surface groups such as carboxyl and hydroxyl can interact strongly with Fe^{3+}. In most instances, Fe^{3+} leads to a decrease in photoluminescence via inner filter effect (IFE) and/or dynamic quenching processes. According to Parambil et al. (2024), CQDs prepared from banana peel material under the thermal condition of 180°C demonstrated specific fluorescent quenching in the presence of Fe^{3+} ions [5].

The effect was achieved with minimal disturbance from other common metal ions. This phenomenon has been attributed to the high charge density and strong Lewis acidity associated with Fe^{3+} ions relative to other metal ions.

Alansari et al. (2025) also demonstrated the effectiveness of green CQDs as fluorescent chemosensors by reporting the detection of both Hg^{2+} and Fe^{3+} using microwave-synthesized CQDs [13]. Across different studies, the reported selectivity, sensitivity, and low detection limits of CQD-based Fe^{3+} sensors indicate that this sensing approach can be reliable and practical for real applications.

2.8.3 Detection of Other Heavy Metal Ions

Apart from Fe^{3+} detection, many more types of heavy metals ions, such as Hg^{2+}, Pb^{2+}, Cd^{2+}, Cu^{2+}, and Cr^{6+}, have been studied for fluorescent sensing using CQDs. The working principle of each sensor relies on the interactions between the respective metal ion and functional groups that decorate the surface of the CQD particles. Since the CQD surface is tunable by altering the synthesis conditions and precursors used, sensors selective to desired analytes can be prepared. Such properties make CQD sensors attractive compared to many traditional analysis techniques.

2.9 Biocompatibility and Other Applications of CQDs

A major advantage that comes with the use of CQDs, particularly the ones synthesized from natural biomass sources, is their excellent biocompatibility and minimal toxicity. In their study on sugarcane bagasse CQDs, Pandiyan et al. (2020) demonstrated their biocompatibility. They also exhibited their antimicrobial characteristics against pathogenic bacteria, making the application of CQDs in medicine more possible [27]. Atchudan et al. (2021) were able to show that banana peel CQDs could be used for in vivo bioimaging and were still non-toxic to organisms and cells[12].

Apart from being used for detection and imaging purposes, the potential of CQDs is further extended to other applications like photocatalysis, LEDs, solar cells, and energy storage devices. For instance, Purwamargapratala et al. (2024) reported the use of banana peel CQDs as an additive in lithium-ion batteries and its potential impact on energy technologies [26].

2.10 Research Gaps and Justification for the Present Study

The reviewed studies show steady progress in the synthesis and application of biomass-derived CQDs. However, some important gaps remain.

First, many hydrothermal synthesis methods used for banana peel-derived CQDs operate at comparatively high temperatures of about 180–200°C [2, 7, 13]. Such conditions require higher energy input, which can reduce the environmental and economic feasibility of the synthesis route. A systematic evaluation of CQDs produced at much lower hydrothermal temperatures, for example at 130°C, is still limited in the literature.

Second, although several banana peel sources have been examined [5], there is not enough reporting on how locally available banana peel varieties affect CQD optical properties and sensing performance when synthesis is carried out under energy-efficient conditions.

Third, the relationship between synthesis temperature, particle size, surface functional group composition, quantum yield, and Fe^{3+} sensing behavior has not been comprehensively clarified for banana peel-derived CQDs synthesized at lower hydrothermal temperatures.

In this work, these gaps are addressed by synthesizing CQDs from banana peel using a low hydrothermal temperature of 130°C. The produced nanoparticles are then characterized using a set of complementary spectroscopic and microscopic techniques, and their performance as fluorescent sensors for Fe^{3+} detection is evaluated. This study supports the development of more energy-efficient, sustainable, and cost-effective methods for preparing functional CQDs with practical analytical applications.

A literature review is a survey of published materials on the topic of interest authored by accredited scholars and researchers. It is quite important to uncover what is already known in the body of knowledge before initiating any research (Hart, 1998). Hence, it is a crucial endeavor for any academic research in theoretical and conceptual progress (Shaw, 1995 and, Webster and Watson, 2002). Thus, it helps to situate your research in the context of what is already known about the topic and find the gap that your research will bridge.

3. Experimental

3.1 Materials

The chemicals used in this study were of analytical grade: ethanol (C_2H_5OH), ferric chloride ($FeCl_3 \cdot 6H_2O$), and distilled water. All of these reagents were purchased from local chemical suppliers in Kathmandu, Nepal. Fresh banana peels (Musa acuminata) were collected from the local market and were used as the only carbon source for the synthesis of CQDs. Banana peel was chosen because it is widely available as an agricultural waste material, contains a variety of naturally occurring components such as cellulose, hemicellulose, lignin, polyphenols, and carotenoids, and fits well with the idea of green and sustainable nanomaterial synthesis [12, 26].

For characterization and preparation, several instruments were used. UV-Vis spectrophotometry was applied for optical characterization of the synthesized CQDs. Fourier Transform Infrared (FTIR) spectroscopy (PerkinElmer Spectrum IR, Version 10.6.2, ASCOL Campus, Kathmandu) was used to identify the functional groups and to understand the surface chemical bonding present in the CQDs. Fluorescence visualization was carried out using a UV chamber fitted with both 365 nm (UVA) and 254 nm (UVC) lamps. A magnetic stirrer was used to prepare the solutions. CQDs were synthesized using a Teflon-lined stainless steel hydrothermal autoclave. After synthesis, the raw materials were dried in a laboratory convection oven. Finally, purification of the CQD dispersion was performed using a 0.22 μm syringe filter.

3.2 Methodology

3.2.1 Raw Material Preparation

The selection and pre-treatment of the carbon precursor are decisive early steps in the bottom-up hydrothermal preparation of carbon quantum dots (CQDs). This is because the chemical and structural composition of the starting biomass determines the surface functional groups, the resulting size distribution, and the photoluminescence behavior of the final CQDs.

Banana peel is a promising biomass precursor due to its wide availability and low cost as an agricultural by-product. It contains substantial amounts of cellulose, hemicellulose, pectin, lignin, and various organic constituents such as flavonoids, polyphenols, and

carotenoids [26]. During hydrothermal carbonization, these components act as internal carbon sources and can also contribute to surface passivation by heteroatom-containing molecules [18]. In addition, natural nitrogen and oxygen atoms present within peel biomolecules can promote "self-doping" of the carbon nanostructures[28]. This self-doping is widely reported to improve photoluminescence quantum yield.

Raw banana peels were first inspected and selected only if they were free from bruising, fungal growth, visible mold, and physical damage. The peels were obtained from a local market in Kathmandu, Nepal. Any damaged or discolored portions were removed completely, since the presence of mold or oxidized tissue can contribute unwanted chemical species. These contaminants could result from fungal secondary metabolites and have the ability to affect the carbonization process by modifying the optical properties of the produced CQDs.

The peels underwent rinsing at least five times with double distilled water after the selection process. The purpose of this rinsing was to eliminate any contaminants on the peels that might arise from pesticides, dust from the soil, and other organic substances. The reason for this rinsing process is that the presence of pesticides on the peelings would mean contamination of the reaction mixture by introducing other elements such as phosphorus and sulfur due to the presence of organophosphates and carbamates.

After washing, the peels were dried by laying them down flat in one layer on aluminium foil. The drying process involved the use of a convection oven maintained at a constant temperature of 50°C for a period of 8 hours. The temperature employed during the drying process was set to enable drying without thermal damage to certain thermosensitive phytochemicals present in the peels. These thermolabile phytochemicals, which include phenolic acids, flavonoids, and carotenoids, are highly prized due to their ability to engage in surface passivation reactions during the hydrothermal synthesis process. It is usually noted that higher drying temperatures, such as those exceeding 80°C, tend to result in a higher rate of volatiles loss and partial destruction of passivating biomolecules. This, in turn, leads to reductions in carbon content and fluorescence quantum yield of the CQDs. Drying of the peels was deemed to be complete once the peel had become brittle and friable.

The dried peel was later powdered in an electric grinding machine made from stainless steel, which worked at very high rotational speed. This process is important because it makes the particle size uniform and small. This is advantageous since it enhances the surface area of the sample to allow for easy dissolution and reaction. The biomass can be carbonized uniformly in the autoclave. Studies have shown that the size of the precursor particles has an effect on CQD properties. Precursors with smaller particles yield CQDs with a narrow distribution, while those with larger precursors may not produce uniformly shaped CQDs.

Figure 3.1: Diagrammatic representation of the preparation of raw material.

3.2.2 Synthesis of Carbon Quantum Dots by Hydrothermal Method

The hydrothermal synthesis technique was chosen as the primary method for preparing CQDs in this study. This selection was based on its established benefits relative to other reported CQD fabrication routes, such as electrochemical ablation, microwave-assisted synthesis, laser ablation, and chemical oxidation methods[29]. In contrast to acid-assisted chemical oxidation methods, which typically rely on concentrated nitric acid or sulfuric acid and generate hazardous liquid effluent, hydrothermal synthesis proceeds without additional chemical reagents. It does not involve the formation of toxic chemical by-products, can use the biomass in its unmodified form as both the carbon source and the surface passivating component, and can be carried out with common laboratory apparatus[30]. The procedure takes advantage of the distinctive physicochemical characteristics of sub-critical hot compressed water. Under sealed-autoclave conditions, when the temperature is maintained in the range of 100 to 200°C, the dielectric constant of water drops markedly compared with its value at room temperature (from about 78 at 25°C to roughly 55 at 130°C). This reduction improves the ability of water to solvate and transport non-polar organic reaction intermediates formed during the process [31]. At the same time, the sealed autoclave produces autogenous pressure, which limits solvent loss and prevents excessive evaporation. As a consequence, the dissolved organic intermediates remain available in a relatively confined environment and stay in close molecular contact. This situation favors a sequence of transformations, including dehydration, polymerization, aromatization, and condensation reactions. Collectively, these pathways lead to the generation of nanoscale graphitic carbon nuclei [32]. A precisely weighed amount of 5 g of dried banana peel powder was introduced into a 150 mL beaker containing 100 mL of double-distilled water. The selected mass-to-volume ratio of 50 mg mL^{-1} was based on earlier optimization experiments. These studies indicated that this concentration is high enough to supply an adequate level of dissolved organic carbon for efficient CQD nucleation, while remaining low enough to avoid early precipitation or uncontrolled aggregation of particles during heating[29, 33]. The mixture was stirred continuously on a magnetic stirrer at 600 rpm for 30 minutes at room temperature. This pre-dissolution and

pre-dispersion stage helps to initiate the dissolution of water-soluble compounds embedded in the peel matrix. These compounds mainly include simple sugars (e.g., glucose and fructose), phenolic acids (e.g., gallic acid and caffeic acid), and short-chain carboxylic acids. Once dispersed into the aqueous phase, these species can act as direct molecular carbon sources during the subsequent hydrothermal treatment [34].

The suspension was stirred continuously on a magnetic stirrer at 600 rpm for 30 minutes at room temperature. This pre-dissolution and pre-dispersion step enhances the initial solubilization of water-soluble phytochemicals from the peel matrix. These components are mainly simple sugars (such as glucose and fructose), phenolic acids (such as gallic acid and caffeic acid), and short-chain carboxylic acids, which later act as direct molecular carbon feedstocks in the hydrothermal reactor [34].

A well-dispersed suspension was then transferred into a 100 mL Teflon-lined stainless-steel autoclave. The autoclave was sealed tightly and placed in a pre-heated muffle furnace. The reaction was carried out at 130°C for a total duration of 12 hours. These hydrothermal conditions were selected for their clear physicochemical justification. At 130°C, the supplied thermal energy is sufficient to exceed the relevant activation barriers for dehydration and condensation reactions of hexose and pentose sugars present in the banana peel biomass. This promotes the formation of intermediates such as 5-hydroxymethylfurfural (HMF) and furfural, which can then undergo intermolecular aldol condensation, aromatization, and cyclization. Through these pathways, polycyclic aromatic structures are generated and serve as the graphitic core precursors of the CQDs [7, 31]. Multiple studies report that temperatures below 120°C lead to incomplete carbonization, producing amorphous nanoparticles with weak and inconsistent photoluminescence. Conversely, temperatures above 180°C can accelerate Ostwald ripening, where larger particles grow at the expense of smaller ones[32]. This typically results in CQDs with broader size distributions and reduced sensing performance.

The reaction time of 12 hours was selected to enable complete and relatively uniform carbonization across the autoclave volume. Reaction times shorter than 6 hours may produce incomplete carbonization, leaving higher concentrations of unreacted organic intermediates in solution. In contrast, reaction times longer than 18 hours may promote progressive agglomeration of newly formed CQDs into larger carbon aggregates. Such aggregates are difficult to redisperse and generally show noticeably reduced fluorescence intensity [35]. Under 130°C in a sealed autoclave, the estimated autogenous pressure (based on the saturation vapor pressure of water at this temperature) is approximately 2.7 atm. This pressure is sufficient to keep the aqueous phase in the liquid state and to minimize evaporative loss of volatile organic intermediates.

After completion, the autoclave was removed from the furnace and allowed to cool naturally to ambient temperature over approximately 2 to 3 hours. Rapid quenching by immersion in cold water was avoided deliberately. Sudden cooling can damage the Teflon liner due to thermal stress and may also trigger faster particle aggregation by disturbing the electrostatic repulsion that stabilizes the developing CQD dispersion during cooling [33]. The resulting product appears as a dark brown to black solution, which is consistent with successful carbonization of the biomass. This color change also suggests the formation of polycyclic aromatic carbon nanostructures decorated with oxygen-containing surface functionalities such as carboxyl (−COOH), hydroxyl (−OH), and carbonyl (C=O) groups [36].

Figure 3.2: Diagrammatic representation of hydrothermal synthesis.

3.3 Purification and Characterization of Carbon Quantum Dots

The crude material collected from the hydrothermal autoclave is a heterogeneous mixture containing the target sub-10 nm CQDs along with incompletely carbonized macroscopic residues, larger carbon aggregates, inorganic salts originating from the mineral fraction of banana peel, and higher-molecular-weight organic intermediates [30]. For this reason, a stringent two-step purification strategy combining high-speed centrifugation and membrane filtration was applied to obtain a more monodisperse and optically uniform CQD fraction appropriate for subsequent spectroscopic measurements and ion-sensing tests [34].

Centrifugation

The dark brown reaction mixture was transferred into centrifuge tubes and centrifuged at 10,000 rpm for 10 minutes at room temperature using a benchtop centrifuge. Under these conditions, dense macroscopic carbon residues, incompletely carbonized particulate matter, and carbon aggregates with sizes greater than approximately 200 nm are effectively sedimented at the bottom of the tube [31]. The supernatant, containing the smaller and well-dispersed CQD fraction, appeared as a clear to slightly turbid reddish-brown solution and exhibited yellowish-green fluorescence under UV irradiation. The supernatant was carefully

decanted with a transfer pipette and retained for additional purification.

Syringe Filtration

The obtained supernatant was then filtered through a $0.22\,\mu$m pore-size syringe filter to remove any sub-micron particulates, residual carbon aggregates, and possible microbial contaminants that could remain after centrifugation. A $0.22\,\mu$m cutoff is commonly used in CQD purification because it retains particles above ~ 220 nm while allowing CQDs to pass. CQDs typically have hydrodynamic diameters in the range of about 2 to 10 nm as determined by dynamic light scattering [24]. The purified CQD dispersion showed a clear yellow-brown appearance in visible light and strong blue-green fluorescence under 365 nm UV excitation. This dispersion was collected in amber glass vials to maintain photoluminescence activity.

Solvent Environment Study

To evaluate how the solvent microenvironment affects the optical response of the prepared CQDs particularly the roles of solvent polarity, hydrogen-bond donor ability, and refractive index the purified CQD stock dispersion was diluted separately in two chemically distinct solvents: (a) analytical-grade ethanol (C_2H_5OH, and (b) distilled water. The same volumetric dilution ratio was used for both solvents so that differences in optical behavior could be attributed only to solvent effects rather than changes in CQD concentration. CQD photoluminescence is known to be highly dependent on the surrounding solvent. This behavior is commonly linked to solvent induced modifications of surface functional group conformations, changes in solvation of the CQD excited state, and hydrogen-bonding interactions between solvent molecules and surface carboxyl and hydroxyl groups on the CQDs [35]. Polar protic solvents such as water and ethanol have been reported to cause a red shift in emission compared with non-polar aprotic media, typically due to stabilization of the excited state dipole via hydrogen bond formation with the CQD surface [37].

UV–Vis absorption spectra were recorded from 200 to 800 nm for all three dispersions: the undiluted CQD stock, the ethanol-diluted sample, and the water-diluted sample. This enabled a controlled comparison of solvent effects on the characteristic electronic absorption transitions of the CQDs [29].

3.3.1 Preparation of Fe^{3+} Stock Solution

Ferric chloride hexahydrate ($FeCl_3 \cdot 6H_2O$; molecular weight) was used as the analytical grade source of Fe^{3+} because it dissolves readily in water, provides a stable solution at the concentrations used in this study, and fully dissociates to generate free solvated Fe^{3+} under conditions that are relevant to biological and environmental contexts [38]. The choice of Fe^{3+} is also motivated by its importance in both environmental monitoring and biomedical

applications. Iron is the most abundant transition metal in the human body and is involved in oxygen transport through hemoglobin, redox catalysis via enzymes. At the same time, excess iron (e.g., haemochromatosis and hepatotoxicity) and iron deficiency (e.g., anemia and impaired cognitive development) can lead to serious health effects [39].

In natural waters, elevated Fe^{3+} levels may result from acid mine drainage, corrosion of iron-based water supply infrastructure, or the release of industrial effluents. Such conditions can promote the formation of reactive hydroxyl radicals through Fenton-type chemistry ($Fe^{3+} + H_2O_2$), creating significant ecotoxicological risks for aquatic organisms and downstream ecosystems [40].

A Fe^{3+} stock solution was prepared by accurately weighing 27 mg of $FeCl_3 \cdot 6H_2O$ using a calibrated analytical balance (precision ± 0.1 mg) and dissolving it completely in 100 mL of double-distilled water in a volumetric flask with gentle magnetic stirring. This procedure produced a stock concentration of approximately 1 mM Fe^{3+}. The stock solution was prepared fresh before each experiment to reduce changes due to hydrolysis and precipitation of ferric hydroxide ($Fe(OH)_3$), which can occur spontaneously in neutral to slightly alkaline aqueous media upon standing—particularly at pH values above 3.0 [38].

Working solutions of 50 μM, 100 μM, and 150 μM were prepared immediately prior to use by volumetric dilution from the stock solution using the standard dilution relation:

$$C_1 V_1 = C_2 V_2 \qquad (1)$$

where C_1 is the stock concentration, V_1 is the volume withdrawn from the stock solution, C_2 is the target working concentration, and V_2 is the final volume of the working solution. The selected Fe^{3+} concentrations reflect ranges relevant to environmental surveillance and clinical diagnostic scenarios. For comparison, the World Health Organization (WHO) guideline value for total iron in drinking water is 0.3 mg L^{-1} (approximately 5.4 μM), which places the studied concentrations within the range typically associated with moderately to severely iron-contaminated water matrices [40].

3.4 Preparation of CQD–Fe^{3+} Samples for Fluorescence Sensing

To systematically examine the fluorescence quenching of the synthesized CQDs with increasing Fe^{3+} concentration, four sample sets were prepared under strictly controlled and identical conditions. The experimental setup was designed so that the total CQD volume and CQD concentration remained constant across all samples. Only the volume and concentration of the added Fe^{3+} working solution were varied. This approach ensures that any observed changes in the optical signal can be attributed directly to the analyte-induced quenching

effect rather than to dilution-induced differences in CQD concentration [38].

CQD-based fluorescence sensing of heavy metal ions can proceed via three major mechanistic routes depending on the specific CQD–metal ion pairing: (i) *static quenching* resulting from ground-state complex formation between the metal ion and CQD surface functional groups, producing non-emissive complexes that reduce the population of fluorescent CQDs; (ii) *dynamic (collisional) quenching*, where diffusion-limited collisions lead to energy transfer from excited CQDs to paramagnetic metal ions; and (iii) the *inner filter effect (IFE)*, where the metal ion solution absorbs excitation light and/or emitted fluorescence before detection [41]. For Fe^{3+}, multiple independent studies indicate that quenching is predominantly governed by a combination of strong inner-sphere coordination between Fe^{3+} and electron-rich surface oxygen-containing groups on the CQDs—especially carboxylate and hydroxyl moieties—forming stable, non-emissive CQD–Fe^{3+} coordination complexes. In addition, an IFE contribution arises because the broad UV absorption band of the $FeCl_3$ solution overlaps substantially with the CQD excitation wavelength region [40].

The four CQD–Fe^{3+} sample sets were prepared as follows:

- **Sample 1 (Blank/Baseline):** 2 mL of purified CQD dispersion was mixed with 0.5 mL of double-distilled water, giving a final Fe^{3+} concentration of 0 μM. This sample provides the reference fluorescence intensity I_0 in the absence of the quenching analyte.
- **Sample 2:** 2 mL of CQD dispersion was mixed with 0.5 mL of the 50 μM Fe^{3+} working solution, corresponding to an effective Fe^{3+} concentration of 10 μM in the final 2.5 mL mixture.
- **Sample 3:** 2 mL of CQD dispersion was mixed with 0.5 mL of the 100 μM Fe^{3+} working solution, corresponding to an effective Fe^{3+} concentration of 20 μM in the final mixture.
- **Sample 4:** 2 mL of CQD dispersion was mixed with 0.5 mL of the 150 μM Fe^{3+} working solution, corresponding to an effective Fe^{3+} concentration of 30 μM in the final mixture.

3.4.1 UV–Vis Spectrophotometric Analysis

UV–Vis absorption spectroscopy was carried out using a double-beam UV–Vis spectrophotometer operating over a wavelength range of 185–1100 nm with a spectral slit bandwidth of 2 nm. Measurements were performed using matched 1 cm path-length quartz cuvettes. The samples—(i) blank CQD dispersion and (ii) three CQD–Fe^{3+} mixtures prepared at progressively increasing Fe^{3+} concentrations—were measured sequentially across 185–400 nm. Baseline correction was done using double-distilled water as the reference blank [29].

For hydrothermally synthesized biomass-derived CQDs, UV–Vis spectra typically show two main electronic absorption features. A strong absorption peak appears in the range

260–275 nm, which corresponds to the $\pi \rightarrow \pi^*$ transition related to aromatic $C = C$ bonds within the sp^2 like graphitic core of the CQDs. A weaker shoulder or secondary band in the range 285–300 nm is commonly associated with the $n \rightarrow \pi^*$ transition of surface oxygen-containing groups such as carbonyl (C=O) and carboxyl (COOH) functionalities [30, 31]. The intensity of this $n \rightarrow \pi^*$ band can be used as a semiquantitative indication of the amount of oxygenated groups on the CQD surface, which act as molecular sites involved in Fe^{3+} sensing [34, 42].

With increasing Fe^{3+} concentration, a reduction in absorbance at the characteristic CQD peaks is expected. This behavior can be explained by two main effects. First, the coordination of Fe^{3+} ions with surface carboxylate groups disturbs the surface electronic environment, thereby weakening the $\pi \rightarrow \pi^*$ absorption. Second, $FeCl_3$ solutions contribute additional broad and largely featureless absorption in the UV region (approximately 200–400 nm), which further reduces the net absorbance recorded for CQDs in the presence of iron ions [38, 43]. Therefore, comparing the four UV–Vis spectra provides spectroscopic evidence for the concentration-dependent interaction between Fe^{3+} and the CQD nanoparticles [40, 44].

3.4.2 FTIR Spectroscopy

FTIR spectroscopy was used to identify and characterize the surface functional groups present on the synthesized CQDs. These groups are important because they influence both the colloidal stability of the CQDs in water (via electrostatic repulsion arising from deprotonated surface carboxylate species) and their Fe^{3+} sensing performance (through coordination and chelation of Fe^{3+} by oxygen-containing surface moieties) [7, 31**?**]. FTIR works by measuring vibrational energy transitions of chemical bonds when they absorb mid-infrared radiation, producing a spectrum that can be interpreted to determine which functional groups are present on the CQD surface [30, 45].

FTIR analysis was performed on purified CQD powder using a PerkinElmer Spectrum IR spectrometer (Version 10.6.2) in Attenuated Total Reflectance (ATR) mode at ASCOL Campus, Kathmandu, Nepal. Before measurement, the CQD aqueous dispersion was evaporated to complete dryness at 60°C on a clean glass substrate to form a solid film. This preparation allowed direct ATR-FTIR measurement without requiring KBr pellet preparation [24, 36]. The FTIR spectrum was collected over 450–4000 cm^{-1}, using a spectral resolution of 4 cm^{-1} and 32 scans averaged to improve the signal-to-noise ratio [32].

The interpreted spectral regions include: (i) a broad band in the 3200–3600 cm^{-1} range attributed to O–H and N–H stretching vibrations, associated with surface hydroxyl groups and adsorbed water, as well as possible amine-related contributions from nitrogen-containing

components originating from the banana peel precursor; (ii) aliphatic $C--H$ stretching bands in the 2850–2960 cm^{-1} region; (iii) carbonyl stretching C=O for carboxylic acid groups around 1700–1740 cm^{-1}; (iv) aromatic ring-related stretching modes such as $C = C$ and C=N in the 1580–1650 cm^{-1} region; and (v) C–O stretching along with O–H bending bands typical of carboxylate-related groups in the 1000–1300 cm^{-1} region [35]. Overall, the observation of oxygen- and nitrogen-containing functional groups is consistent with the chemical composition of the banana peel precursor and matches previously reported FTIR assignments for hydrothermally synthesized biomass-derived carbon quantum dots [33].

4. Result and Discussion

4.1 Material Synthesis

Carbon quantum dots (CQDs) were successfully synthesized from banana peel waste using the hydrothermal method. Banana peel is an abundantly available agricultural by product whose chemical composition rich in carbohydrates, polyphenols, flavonoids, tannins, and various heteroatom-containing organic molecules makes it a particularly well-suited natural carbon precursor for CQD synthesis[12].The primary driving motivation for using banana peel as a precursor is that it provides both the carbon and heteroatom (nitrogen, oxygen) sources simultaneously, without requiring any additional chemical reagents or surface-passivating agents. This makes the entire synthesis route green and environmentally benign, which is increasingly recognized as a significant advantage in nanomaterial fabrication[46]. The hydrothermal method was selected specifically because it is one of the most widely adopted and reproducible synthesis routes for biomass-derived CQDs. Unlike chemical oxidation-based or arc-discharge methods, hydrothermal synthesis does not rely on toxic reagents such as concentrated nitric acid or strong oxidants, and it operates entirely in an aqueous medium [47]. The method also allows relatively good control over particle size, surface chemistry, and the degree of carbonization, all of which directly influence the fluorescence properties of the resulting CQDs [47]. Several previous reports have established the hydrothermal method as a reliable approach for producing photoluminescent CQDs from banana peel specifically, typically yielding particles in the 2–10 nm range with well-defined optical characteristics [12].

4.2 Mechanism of Hydrothermal Synthesis

In the case of hydrothermal synthesis method, first step involves the sealing of the banana peel precursor solution in a stainless-steel autoclave in an environment of high temperature in the range of 160-220 °C. As the result of being in high temperature environment, the water present becomes highly reactive sub-critical water due to which increased molecular mobility and ionic dissociation of organic molecules occurs. This creates a uniquely favorable environment for the decomposition and transformation of complex biomolecules such as polysaccharides, polyphenols, and proteins present in the banana peel matrix. The organic matter undergoes a series of progressive chemical reactions under hydrothermal conditions. Initially, the high temperature induces dehydration of polysaccharides (e.g., starch, cellulose,

hemicellulose), cleaving glycosidic bonds and generating simpler carbonaceous intermediates such as furans and organic acids [48]. These intermediates then undergo further polymerization and cross-linking, forming three-dimensional aromatic networks that constitute the graphitic cores of the nascent CQDs. Simultaneously, nitrogen and oxygen from the amino acids, amides, and phenolic groups present in the banana peel become incorporated into this developing carbonaceous framework, endowing the resulting CQDs with heteroatom-doped surface chemistries that are critical for their fluorescence behavior [46]. Crystal growth in the hydrothermal system follows two primary mechanisms: Ostwald ripening and oriented attachment. In Ostwald ripening, thermodynamic instability drives the dissolution of smaller, high-surface-energy nanoparticles and the subsequent redeposition of their constituent matter onto larger, more stable particles [49]. This process progressively narrows the size distribution of the CQD population over time and tends to produce larger, more crystalline particles with extended hydrothermal reaction times. Oriented attachment, on the other hand, involves the direct collision and fusing of adjacent primary nanocrystals along energetically favorable crystallographic faces, driven by the minimization of interfacial free energy[49]. In hydrothermal nanoparticle synthesis, both mechanisms often operate in parallel, with oriented attachment generally dominating in the earlier stages of growth and Ostwald ripening becoming more significant as the reaction proceeds [49]. The final morphology and size of the CQDs is therefore a product of the balance between these two growth pathways, which is influenced by reaction temperature, reaction duration, and the initial concentration of the precursor solution. The high-pressure environment inside the autoclave also promotes the surface passivation of the carbon cores, leading to the formation of abundant surface functional groups. The oxygen-rich environment derived from the banana peel's hydroxyl and carboxyl groups causes the CQD surfaces to become densely functionalized with hydroxyl (-–OH), carboxyl (-–COOH), and carbonyl ($C = O$) groups [46]. These oxygenated surface states play a dual role: they render the CQDs highly water-dispersible, and they serve as the active coordination sites responsible for the sensing behavior toward metal ions, particularly Fe^{3+} , which is discussed in detail in section 4.3.

4.2.1 Electron Transfer Mechanism of Fe^{3+} Sensing

The fluorescence quenching of the synthesized CQDs in the presence of Fe^{3+} ions arises from a combination of mechanisms, predominantly static quenching and photo-induced electron transfer, both of which are facilitated by the interaction between Fe^{3+} and the oxygen-containing surface functional groups of the CQDs[50]. In the static quenching mechanism, Fe^{3+} ions form stable, non-emissive ground-state complexes with the carboxyl and hydroxyl groups on the CQD surface through inner-sphere coordination. The oxygen donor atoms in

these functional groups donate lone electron pairs to the partially filled 3d orbitals of Fe^{3+} , forming stable chelate complexes that effectively remove emissive CQD species from the excited-state pathway [51]. In static quenching, the fluorescence lifetime of the remaining uncomplexed CQDs stays essentially unchanged, while the overall emission intensity decreases proportionally with increasing quencher concentration because the emitting population itself is reduced. This is in contrast to dynamic (collisional) quenching, in which the excited CQDs and the Fe^{3+} ions interact during the brief excited-state lifetime, returning the CQD to its ground state without photon emission through non-radiative deactivation [18]. In practice, both static and dynamic quenching have been reported for CQD–Fe^{3+} systems, and many studies report that both mechanisms operate concurrently [50].

The paramagnetic nature of Fe^{3+} (possessing five unpaired 3d electrons) is also a key factor in its exceptional quenching efficiency. Upon photoexcitation of the CQDs, electron-hole pairs are generated within the carbon core. The excited electrons, rather than recombining radiatively to emit photons, can transfer to the energetically accessible 3d orbitals of the coordinated Fe^{3+} , which acts as an electron acceptor[52]. This photo-induced electron transfer (PET) process suppresses radiative recombination, thereby quenching the fluorescence. The highly positive reduction potential ofFe^{3+} /Fe^{2+} makes Fe^{3+} thermodynamically favorable as an electron acceptor from the excited CQDs, which explains its substantially stronger quenching efficiency compared to other divalent and monovalent metal ions that do not have accessible, low-energy unoccupied orbitals [18]. In addition to these mechanisms, the inner filter effect (IFE) has been proposed as a contributing factor to the observed quenching in some CQD-Fe^{3+} systems. The IFE arises because Fe^{3+} has a broad UV absorption that overlaps significantly with the excitation wavelengths of the CQDs, meaning that a portion of the incident excitation light is absorbed by the Fe^{3+} ions before reaching the CQD fluorophores, and a portion of the emitted light may similarly be reabsorbed [53]. While the IFE alone can account for some fluorescence attenuation, the strong quenching observed at even modest Fe^{3+} concentrations and the high selectivity of the CQD response for Fe^{3+} over other ions confirm that the primary mechanisms are electron transfer and complex formation rather than the IFE alone [50].

4.3 Characterization

Following synthesis, the CQD solutions were characterized using three complementary techniques: visual inspection and fluorescence imaging under a UV chamber, UV-Vis absorption spectrophotometry, and Fourier transform infrared (FTIR) spectroscopy. Each technique probed different aspects of the CQD structure their fluorescence behavior, electronic transitions, and surface chemistry, respectively.

4.3.1 UV Chamber Fluorescence Analysis

. Immediate and qualitative evidence of the success of CQD synthesis came from observations made using a UV chamber. The CQD solutions obtained through synthesis were observed under three different forms of light illumination, which included white light, UV light of wavelengths of 365 nm (UVA) and 254 nm (UVC). Observations made under normal light conditions revealed that the solutions had a faint yellowish brown appearance, similar to that of concentrated CQD solutions derived from biomass and with some precursor present [5]. However, upon UV irradiation, the solutions exhibited blue-green photoluminescence, which is the hallmark of successfully synthesized photoluminescent CQDs. Under 365 nm (UVA) illumination, the as-prepared, unfiltrated CQD suspension exhibited fluorescence; however, the intensity of the emission was relatively weak and slightly scattered. Such observation has been reported in freshly prepared unfiltrated CQD suspensions from biomass and is due to the inner filter effect because of the high concentration of absorbing agents such as organic moieties, polyphenolic compounds, and carbonaceous aggregates competing for the incident light with CQDs [5]. These impurities trap the UV light and then emit it back at a longer wavelength or convert it to heat energy, reducing the overall intensity of emissions from the CQDs. In order to enhance the fluorescence behavior, the solution was filtered and further diluted using ethanol as well as distilled water separately, yielding two diluted samples. The ethanol-diluted sample of the CQDs exhibited significantly more pronounced blue-green fluorescence than the undiluted sample. This is because the dilution has an effect of reducing the inner filter effect, where the reduced total concentration means that more light will be able to reach the fluorophores within the CQDs. In addition, there is an effect attributed to the solvent, where the polarity of the ethanol used affects the hydrogen bond networks surrounding the CQD groups, thus reducing interaction between the particles and subsequent fluorescence quenching [7]. On the other hand, the emission behavior of the sample diluted with water was observed to be somewhat different from that of the sample diluted with ethanol. Since water is a very polar protic solvent, hydrogen bonding between the surface functional groups of the CQDs and the solvent is more pronounced. It influences the solvation shell around the CQDs and the energy gap of surface trap states [7].The polarity of the environment is well known to be one of the parameters that affect the fluorescence characteristics of the CQDs, and this can clearly be seen from the difference observed between the two dispersion media. Further analysis were performed on the UV chamber with visual inspection for the effect of increasing amounts of Fe^{3+} ions on the quenching properties of CQDs (0, 50, 100, and 150 μM), in addition to short wave UV light exposure (254 nm, UVC). The undoped sample showed the highest brightness of the green fluorescence emission,

verifying the photoluminescence property of the produced material. However, when there was a progressive increase in Fe^{3+} concentration from 50 μM to 100 μM and 150 μM, an observable decrease in fluorescence intensity was noticed without the use of any instrument. The most significant decrease in fluorescence intensity was seen from 100 μM to 150 μM which correlated to 22.8% and 31.8% quantum efficiencies determined by UV-Vis. The almost total quenching seen at concentrations as high as 150 M Fe3+ suggests a case where the CQDs approach saturation with respect to the binding capacity of the surface sites, and this qualitative observation further supports the quantitative results presented in Section 4.3. A similar dependence of the visual quenching on concentration has also been shown in banana peel-based CQDs [5] and other biomass-based CQD sensors [**?**].

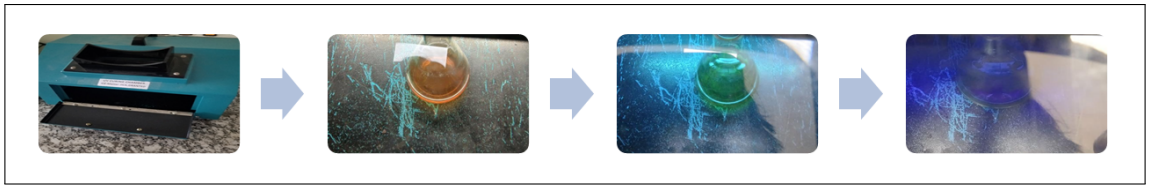

Figure 4.1: Carbon quantum dots under normal daylight, 365nm uv light and 254 nm uv light respectively.

Figure 4.2: Carbon quantum dots solution under uv lamp.

Figure 4.3: Ethanol diluted Carbon quantum dots solution under uva lamp.

Figure 4.4: Distilled water diluted Carbon quantum dots solution under uva lamp.

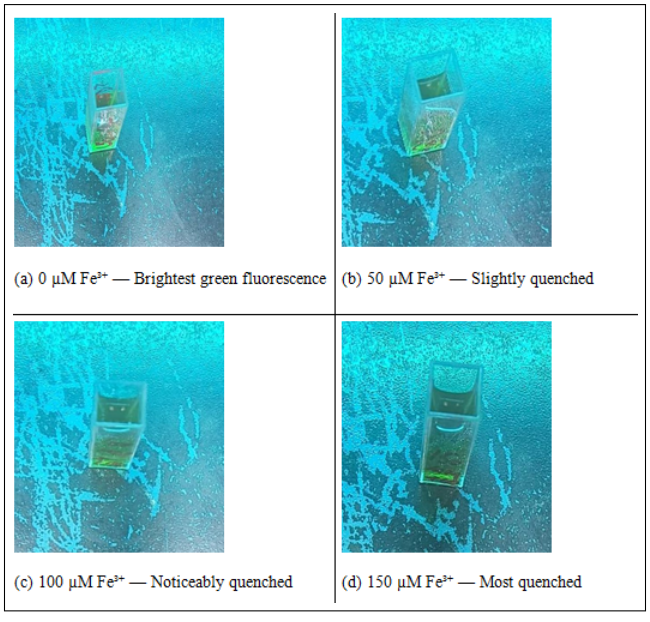

Figure 4.5: Photographs of CQD solutions with 0, 50, 100, and 150 μM Fe^{3+} under short-wave UV irradiation (254 nm).

4.3.2 UV-Vis Spectrophotometric Characterization

Ultraviolet-visible (UV-Vis) absorption spectroscopy is a fundamental technique for characterizing the electronic structure and optical transitions of CQDs. The absorption spectra of CQDs characteristically display two types of transitions: $\pi \rightarrow \pi^*$ transitions arising from the sp^2–hybridized carbon network within the graphitic core of the dots, which typically produce peaks in the 225–270 nm range, and $n \rightarrow \pi^*$ transitions involving lone pairs on oxygen-containing surface functional groups ($C = O$, –COOH, —OH), which give rise to weaker shoulders or secondary peaks in the 270–400 nm range [54].These characteristics depend on the surface chemistry, heteroatom doping, the solvent used, and the level of graphitization of the CQDs.

Three samples of the CQDs were characterized; these include the undiluted solution, the ethanol diluted solution, and the distilled water diluted solution. There were variations in the absorption characteristics of each of these samples based on their solvent media and concentrations. The absorption spectrum of the ethanol-diluted CQD solution exhibited a sharp peak between 225 and 230 nm with an absorption value of 0.293 a.u., which was attributed to $\pi \rightarrow \pi^*$ transitions in the aromatic carbon skeleton. After this main peak, the absorbance dropped gradually from 250 to 400 nm, indicating weaker $n \rightarrow \pi^*$ transitions in the oxygen-functionalized surface groups. The reason behind the relatively lesser absorption value of the ethanol-diluted sample compared to the aqueous samples is the partial breaking of hydrogen bonding between the particles due to ethanol. Ethanol binds with the hydroxyl and carboxyl functional groups on the CQD particle surface, thus minimizing the particle agglomeration effect and hence decreasing the optical density [7]. In this case, the sample diluted in distilled water showed a marked absorption peak around 200 nm, characterized by the high maximum absorbance value of 0.88 a.u., caused again by $\pi \rightarrow \pi^*$ transitions, together with an absorption shoulder from 250 to 300 nm, due to $n \rightarrow \pi^*$ transitions. This is supported by the much higher total absorbance of the aqueous suspension compared to the ethanol-based one, which can be attributed to the stronger interaction between particles and hydrogen bonding enabled by water. Water molecules form extensive hydrogen bonding networks with the –OH and –COOH groups on the CQD surface, which can enhance effective light scattering and increase apparent absorbance [7]. This solvent-dependent variation in optical properties is well-established for hydrophilic CQDs and has been reported by multiple groups working with biomass-derived materials [5]. The pure CQD solution had an average absorbance peak value of 0.646 a.u. near 200 nm, with a slow decline from 260 to 800 nm for the $n \rightarrow \pi^*$ transition of oxygenated functional groups.Intermediate absorbance reading, between those obtained from the solutions of distilled water and ethanol, is ascribed to both

the elevated concentration of CQDs and organic fragments left after the synthesis process, contributing to extra absorption and scattering. These residual impurities are well-known limitations in the hydrothermal synthesis of bio-based carbon quantum dots and the reason behind the non-monotonic relationship between absorbance and dilution in varying solvents [49].

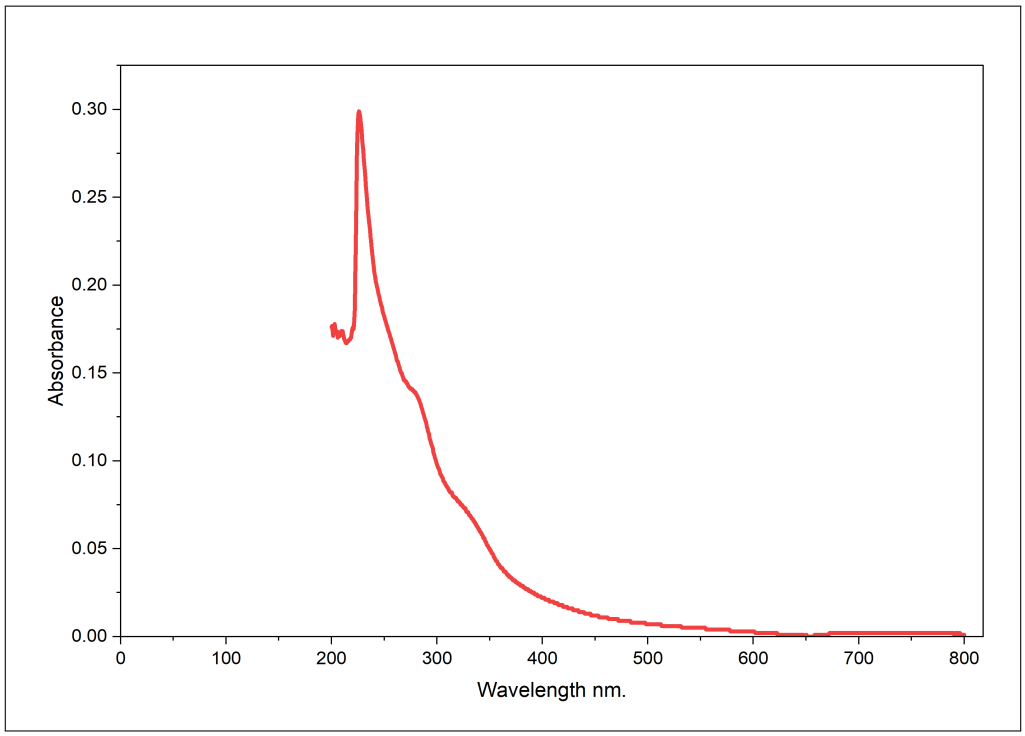

Figure 4.6: Absorbance VS Wavelength of sample diluted with ethanol.

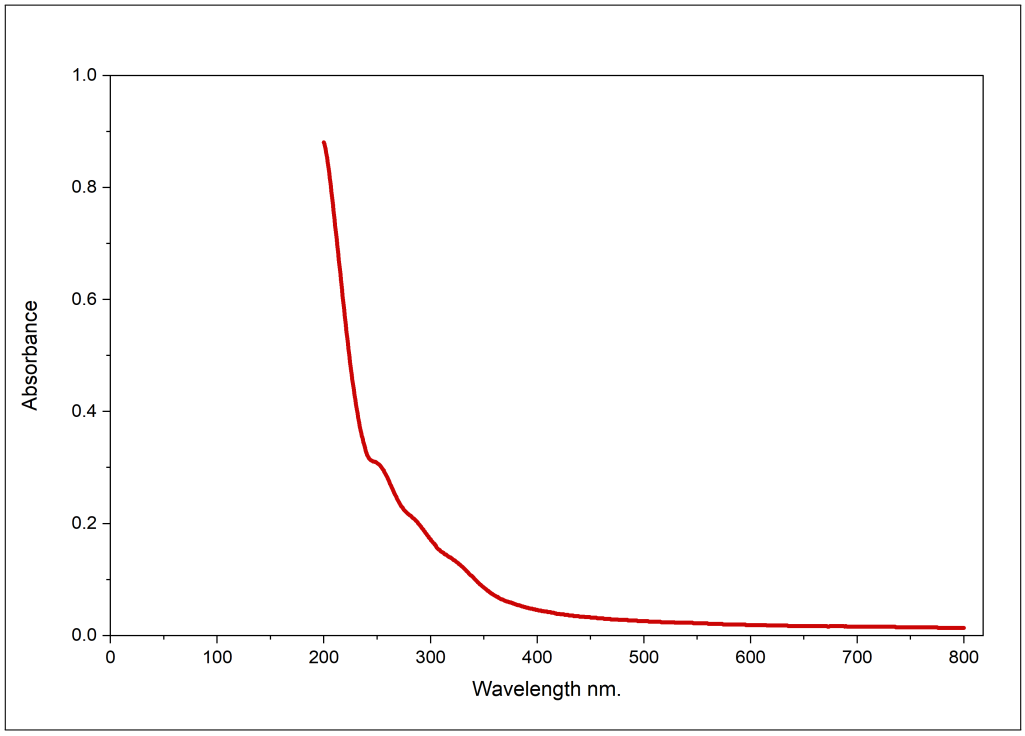

Figure 4.7: Absorbance VS Wavelength of sample diluted with distilled water.

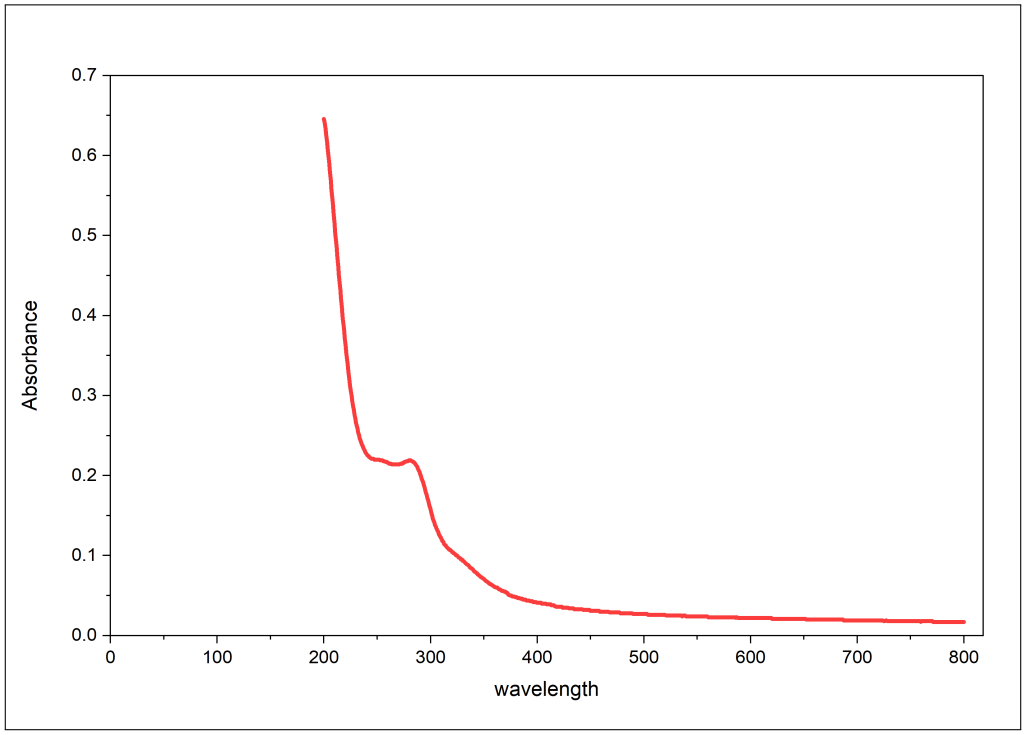

Figure 4.8: Absorbance VS Wavelength of Undiluted CQDs.

4.3.3 FTIR Characterization

To study the functional groups of the CQDs prepared, Fourier Transform Infra-red Spectroscopy (FTIR) was conducted. The FTIR technique plays an important role in studying surface functional groups of biomass-based CQDs due to its direct chemical evidences in relation to the presence of functional groups responsible for their dispersability in water and the ability to detect metal ions [55]. For the FTIR spectrum obtained, the wavenumber range used is 450-4000 cm^{-1}, in which several characteristic absorption peaks are noted. Among these, the most significant one occurs at 3334.1 cm^{-1} and can be associated with $O-H$ bond vibration on the surface of hydroxyl groups and/or $N-H$ vibration of amine/amide groups. The extensive nature of this peak arises from the hydrogen-bonding environments of the said groups on the surface of the CQDs. The existence of –OH groups is in line with the high concentration of oxygen present in the banana peels used as the precursor, as well as the common property of biomass-based CQDs [55]. The hydroxyl groups play an essential role in providing hydrophilic properties to the CQDs and, consequently, maintaining their stable dispersion in aqueous environments. The peak at 2974 cm^{-1} relates to the stretching vibrations of aliphatic $C-H$, confirming the existence of unaromatized sp^3 carbon-rich organics from the initial banana peel raw material that remain after the hydrothermal treatment process. This band has similarly been identified in the FTIR spectra of CQDs obtained from banana peels by Atchudan et al. [12] and Parambil et al.[5]. The prominent peak located at 1732.2 cm^{-1} corresponds to the stretching vibration of $C=O$ present in carboxylic acid groups (-COOH). It is possibly the most analytically important band on the whole spectrum since the carboxyl group is the main site where chelation of Fe^{3+} occurs through an inner sphere complex. Multiple oxygen donor atoms in the carboxylate moiety (–COO) provide a favorable geometry for Fe^{3+} complexation, and the strength of this complexation directly governs the sensing selectivity and quenching efficiency of the CQDs [52]. The presence of a strong carboxyl peak at this position is consistent with the oxidizing environment within the hydrothermal autoclave, which promotes the oxidation of primary alcohols and aldehydes derived from the carbohydrate breakdown to carboxylic acid groups. The peak at 1609.9 cm^{-1} is assigned to aromatic $C=C$ stretching and/or N–H bending vibrations, the latter indicative of nitrogen incorporation into the CQD framework from nitrogen containing species in the banana peel (e.g., amino acids, amides). Nitrogen containing functional groups in CQDs are known to enhance photoluminescence quantum yield and modify the surface charge density, both of which are beneficial for sensing applications [48]. The bands at 1369.99 cm^{-1} and 1318.1 cm^{-1} are attributed to C–N stretching or C–O–H bending vibrations, further corroborating the co-presence of nitrogen-containing and oxygen-containing

surface functionalities. The cluster of peaks at 1160.7, 1100.2, and 1031.57 cm^{-1} are attributed to C–O–C stretching vibrations of ether linkages or epoxide groups. Such linkages commonly arise from the condensation and dehydration of carbohydrate-derived intermediates during hydrothermal carbonization and are consistently observed in FTIR spectra of CQDs derived from carbohydrate-rich biomass precursors [[46]. The peaks in the fingerprint region between 400 and 900 cm^{-1} (at 819.29, 668.36, 535.15, 482.44, and 458.30 cm^{-1}) are associated with aromatic $C–H$ out-of-plane bending and lattice vibrations characteristic of the residual banana peel carbonaceous framework. Overall, the FTIR spectrum is in excellent agreement with previously reported spectra for banana peel-derived CQDs [5] and is consistent with published data on hydrothermal CQDs derived from other carbohydrate-rich biomass precursors [48]. Critically, the spectrum provides unambiguous molecular-level evidence for the carboxyl and hydroxyl groups that are theorized to act as the primary Fe^{3+} chelation sites in the sensing mechanism described in section 4.1.2.

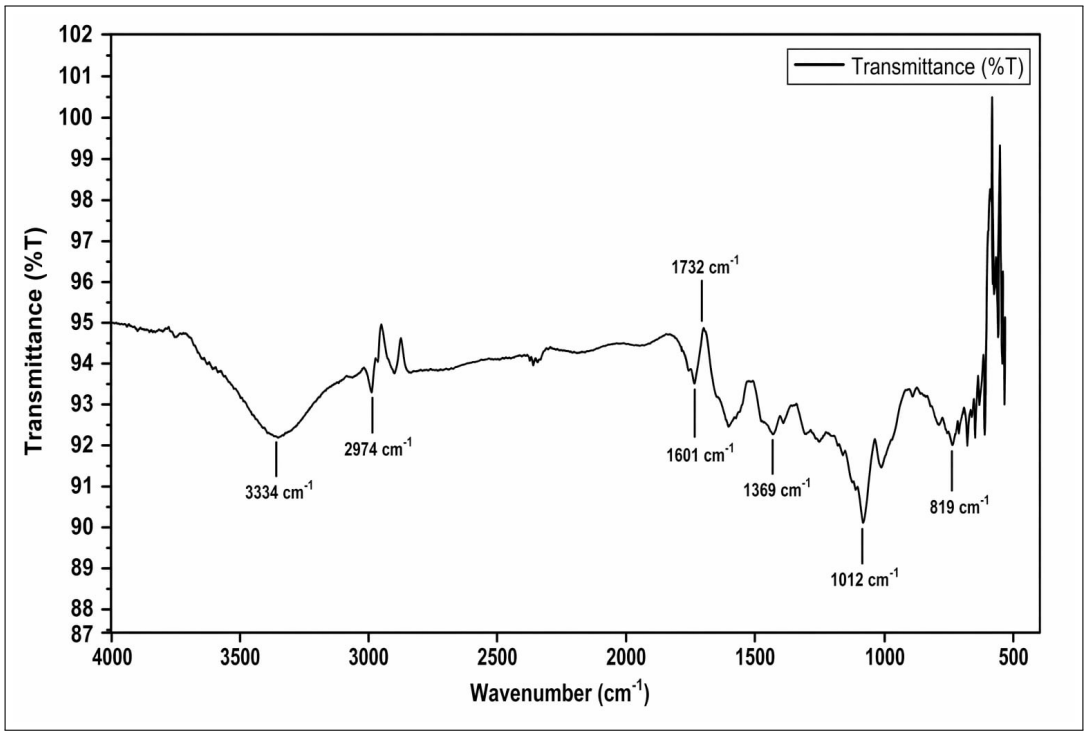

Figure 4.9: FTIR spectrum of CQDs synthesized from banana peel.

4.4 Application: Fe^{3+} Sensing

The sensing capability of the synthesized CQDs toward Fe^{3+} was evaluated by recording the UV-Vis absorbance spectra of CQD samples after addition of Fe^{3+} at four concentrations: 0, 50, 100, and 150 μM. The spectra revealed two consistent spectral features across all samples: a shoulder at approximately 270 nm attributed to $\pi \rightarrow \pi^*$ electronic transitions

of the sp^2 hybridized carbon core, and an absorbance peak at 285.5 nm corresponding to $n \rightarrow \pi^*$ transitions of surface functional groups including $C = O$, -–OH, and -–COOH [54]. The analytical wavelength of 285.5 nm was chosen based on the results of systematic and monotonous dependency of the absorbance on the increase in Fe^{3+} concentration. The absorption value for the case of pure CQDs (0 μM Fe^{3+}) at 285.5 nm was recorded at 1.041 a.u. After adding 50 μM Fe^{3+} to the sample, the absorbance value decreased slightly to 0.989 a.u., resulting in a quenching percentage of about 5%. The relatively low quenching effect at 50 μM means that the Fe^{3+} is bound to a portion of CQD surface sites at this concentration.It is clear that the degree of quenching increased dramatically at 100 μM Fe^{3+}, with an absorbance of 0.804 a.u., equivalent to a quenching efficiency of 22.8%. Thus, a considerable rise in the quenching degree from 5% at 50 μM to 22.8% at 100 μM can show that the system works within a more sensitive quenching degree range, whereby the number of occupied CQDs surface states is more compared to electron transfer/complex forming processes. The lowest absorbance value of 0.710 a.u., indicating the highest percentage quenching of 31.8%, occurred at 150 μM Fe^{3+}. The sub-linear progression of quenching efficiency — from 5% at 50 μM to 22.8% at 100 μM to 31.8% at 150 μM — is consistent with the saturation behavior expected for a surface coordination-based sensing system. As the Fe^{3+} concentration approaches the level at which most available CQD surface binding sites are occupied, the incremental quenching per unit increase in Fe^{3+} concentration decreases, since there are fewer unoccupied sites available for new complex formation. This pattern is commonly described by Stern-Volmer-type quenching kinetics in which the response curve shows a linear region at low quencher concentrations followed by a departure from linearity at higher concentrations, often interpreted as evidence of a combination of static and dynamic quenching or of site saturation [11,12]. The UV-Vis absorbance-based sensing approach used in this study, while somewhat less sensitive than photoluminescence-based measurements, offers certain practical advantages. Absorbance measurements are generally more robust to environmental interference and less susceptible to inner filter effects, which can distort PL-based measurements in high-concentration analyte systems. The monotonic decrease in absorbance at 285.5 nm across the tested Fe^{3+} concentration range provides a straightforward quantitative relationship between Fe^{3+} concentration and optical response that is well-suited for analytical sensing applications.

4.4.1 Summary of Spectral Parameters

The UV-Vis spectral parameters at each Fe^{3+} concentration are summarized in Table 4.1.

Table 4.1: Summary of UV-Vis spectral parameters at each Fe^3+concentration

S.N.	Sample	Peak Abs. (285.5nm)	Quenching
1	CQDs Only	1.041	-
2	CQDs + 50μM Fe^{3+}	0.989	5 %
3	CQDs + 100μM Fe^{3+}	0.804	22.8 %
4	CQDs + 150μM Fe^{3+}	0.710	31.8 %

Quenching percentage calculated as

$$Q(\%) = \frac{A_0 - A_x}{A_0} \times 100 \tag{4.1}$$

where,$A_0 = 1.041$ (baseline absorbance at 0 μM Fe^{3+}).

where $A_0 = 1.041$ (baseline absorbance at 0 μM Fe^{3+} and $A_0 is the absorbance at a given concentration. Thi$ *basedionsensingstudies*[50].

4.4.2 Individual Absorption Spectra

The UV-Visible spectrum for the CQD alone solution (0 μM Fe^{3+}) showed an absorption peak at 285.5 nm with a value of absorbance being 1.041 a.u. Such an observation is indicative of the sp^2 hybridization of carbon domains and presence of oxygen functional groups on the surface of the CQDs. These results are in close correlation with previously published studies on the UV-Visible analysis of banana peel-derived CQDs done by Atchudan et al.[12] and Parambil et al.[5]. Both studies have reported an absorption band in the 270-290 nm range.

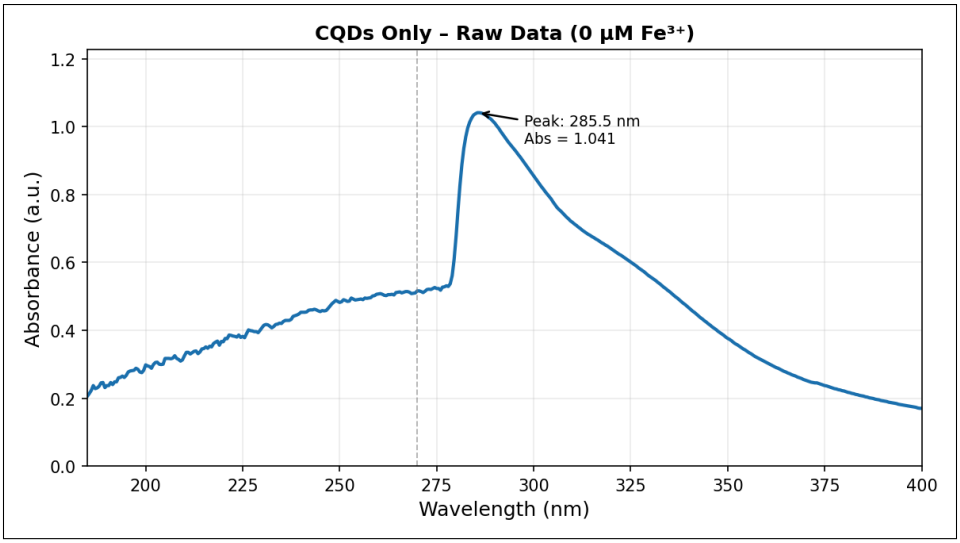

Figure 4.10: UV-Vis absorbance spectrum of CQDs only (0 μM Fe^{3+})

With the addition of 50 μM Fe^{3+}, there was a slight reduction in absorbance to 0.989 a.u., which translates to around 5% quenching. This low decrease in absorbance could be explained by the first step of interaction between Fe^{3+} ions and available surface binding sites. Only a small number of binding sites have been saturated at this concentration, thus giving rise to only a minor effect on absorbance. Therefore, from this result, it can be seen that the detection limit of the CQD using absorbance in the UV–Vis range is somewhere around or below 50 μM.

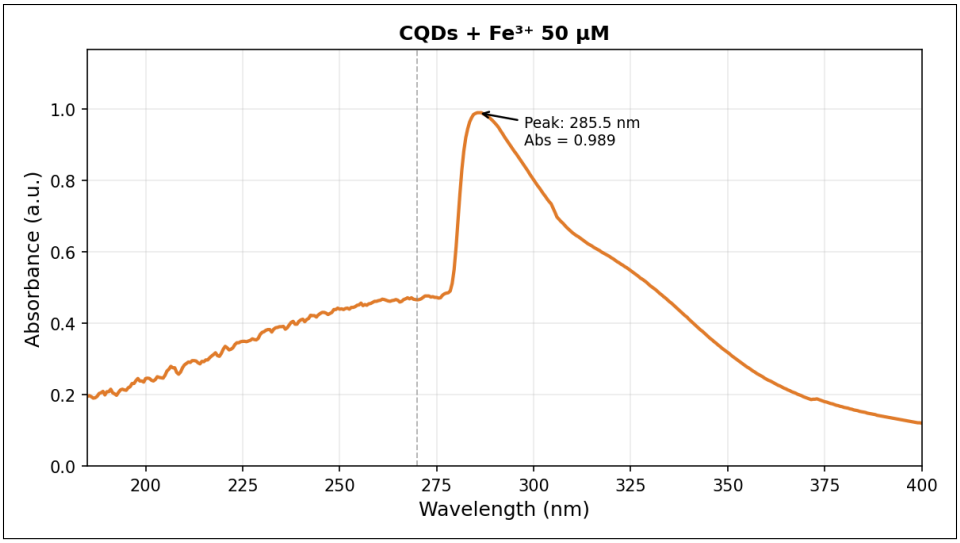

Figure 4.11: UV-Vis absorbance spectrum of CQDs + 50 μM Fe^{3+}

A more substantial drop in absorbance occurred at 100 μM Fe^{3+}, with a value of 0.804 a.u., which corresponds to 22.8% of the absorbance decrease compared to the control value. The abrupt reduction from 50 to 100 μM suggests that the specified range is highly sensitive; here, an increase in the concentration of Fe^{3+} leads to a relatively significant decrease in absorbance. At the same time, this range should coincide with the linear part of the Stern–Volmer plot, which is optimal for the quantitative analysis [18]. The stronger quenching effect can be attributed to the larger interaction between Fe^{3+} and the surface binding sites.

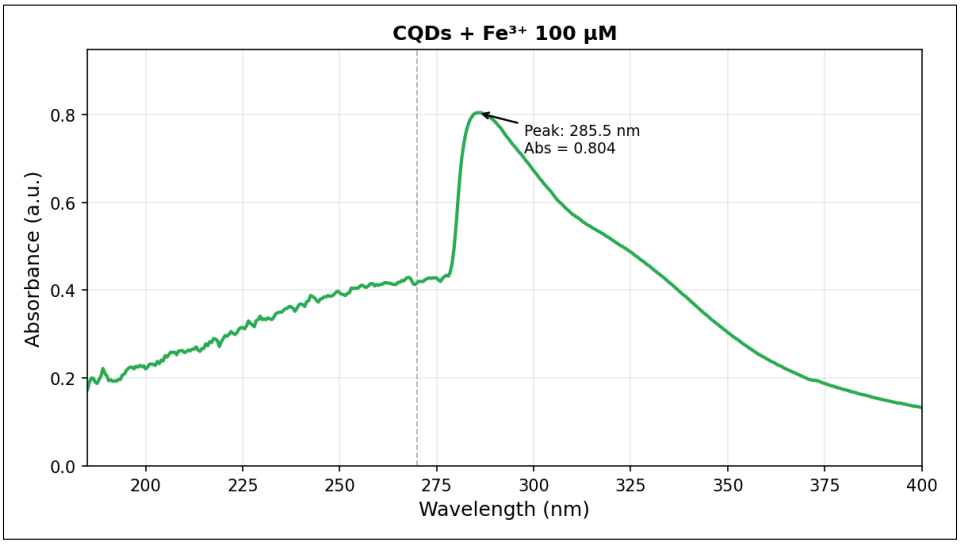

Figure 4.12: UV-Vis absorbance spectrum of CQDs + 100 μM Fe^{3+}

Under the condition of increased concentration at 150 μM Fe^{3+}, the absorbance dropped to 0.710 a.u. and thus corresponded to 31.8% of quenching, which is the highest percentage obtained from the experiment. Nonetheless, the decrease in absorbance from 100 to 150 μM is relatively minor compared to the decrease in absorbance from 50 to 100 μM (around 9% and 18%, respectively), which suggests that the quenching process reached its saturation point. In this case, all the binding sites of high affinity in the CQD surface are probably filled up, and the rest of Fe^{3+} ions bind to low affinity sites. This trend reflects the limited number of available surface coordination sites and is consistent with previously reported behavior for CQD-based sensing systems [46].

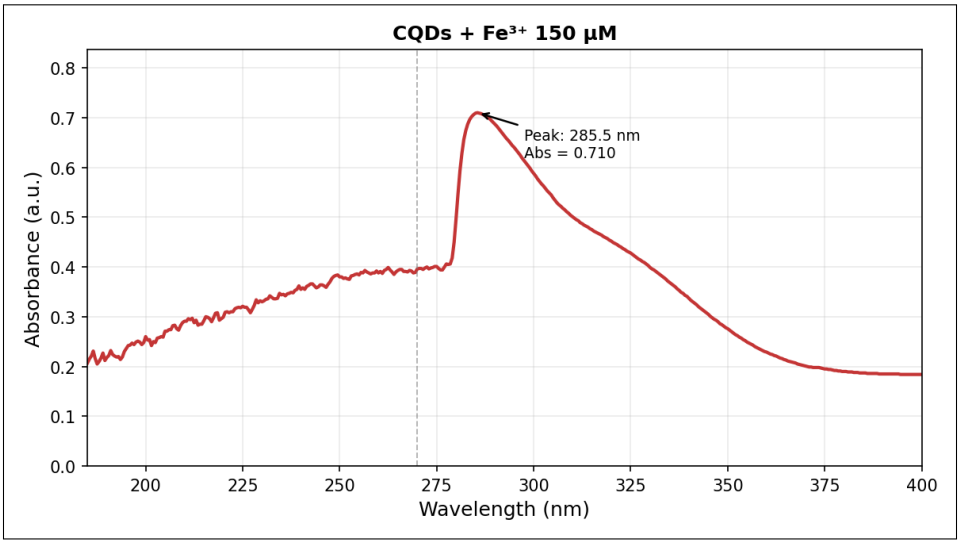

Figure 4.13: UV-Vis absorbance spectrum of CQDs + 150 μM Fe^{3+}

4.5 Conclusion

The CQDs were prepared from the banana peel waste through a facile hydrothermal treatment method conducted at 130 °C for 12 hours without the use of any hazardous chemicals or surface passivation agents. The use of the banana peel waste as the source material is justified because it contains high levels of carbohydrates and polyphenols that not only facilitate carbon formation but also help in the creation of functional groups necessary for photoluminescence.

The synthesis of CQDs was validated using UV chamber analysis, UV–Visible spectrometry, and FTIR spectrometry. There were blue-green emissions of light observed from the material during exposure to UV light. The UV–Visible spectrum had a shoulder at 270 nm resulting from $\pi \rightarrow \pi^*$ electron transitions, as well as a maximum at 285.5 nm that resulted from $n \rightarrow \pi^*$ electron transitions; these transitions characterize oxygen-containing CQDs. The FTIR showed that there were hydroxyl (–OH), carbonyl (C=O), aromatic C=C, and ether (C–O–C) functional groups present in the surface of the CQDs.

Fe^{3+} detection was carried out through the UV–Visible absorbance test. It was noted that there was a steady reduction in absorbance values at 285.5 nm upon increment in Fe^{3+} concentrations. Quenching efficiency was 5%, 22.8%, and 31.8% for 50, 100, and 150 μM, respectively. The highest variation was recorded in the interval from 50 to 100 μM, which shows that this concentration range is the best for detection purposes. As the concentration of Fe^{3+} further increases, there was little variation, which could be attributed to the saturation of binding sites on the CQDs' surface. Considering that the tests were based on absorbance, the quenching efficiency is considered low; more pronounced results would be.

5. Limitations and Future enhancement

5.1 Limitations

Perhaps the most consequential constraint of this work was the unavailability of a fluorescence spectrophotometer, which meant that Fe^{3+} sensing had to be evaluated entirely through UV-Vis absorbance measurements.It is a relatively insensitive detection method compared to photoluminescence spectroscopy; hence, the measured quenching efficiencies of 5%, 22.8%, and 31.8% for 50, 100, and 150 μM Fe^{3+} concentrations, respectively, may be underestimated since they represent just a small part of the true interaction between the CQDs and Fe^{3+}. Apart from that, the lack of information about the fluorescence spectra precluded calculating essential analytical parameters like the LOD, linearity range, and Stern–Volmer quenching constants.

In regards to the characterization of the CQDs physically, structurally and spectroscopically, this study also lacked in areas. It should be noted that since the synthesis method used by these authors does not employ transmission electron microscopy (TEM), it became impossible to confirm whether the particles obtained are indeed very small and uniform in size, two factors which have significant impact on the properties of these particles when it comes to sensing applications. In addition to that, there was no use of X-ray diffraction (XRD) analysis which would have revealed how ordered the carbon cores are within this structure. Another factor, the quantum yield of the CQDs, was not calculated and thus remains unknown.

Two more gaps should be pointed out. The first one is that no selectivity studies were performed; thus, the question of whether the quenching behavior shown is really selective towards Fe^{3+} or whether there would be a similar effect for the other metal ions contained in environmental samples like Cu^{2+}, Pb^{2+}, Al^{3+}, Cr^{3+}, or Hg^{2+} remains open. The second one is that all detections were done on Fe^{3+} standards in laboratory conditions; hence, the performance of the CQDs in an actual sample of water with its different pH values, organic matter concentration, and metal ions is left unanswered by the paper.

5.2 Future Enhancements

The immediate next task that needs to be carried out in continuation of this study should therefore be quite clear – carry out the sensing experiment again but using the fluorescence spectroscopy technique this time. The PL-based detection of the exact same CQD Fe^{3+}

compound will provide us with the LOD, the Stern Volmer quenching constants, and the right linear range of calibration, thereby allowing us to compare our results with the vast literature on CQD sensing via fluorescence spectroscopy.

In terms of characterization, TEM imaging should be a priority to ensure that the nanoparticles' dimensions are confirmed at the nanometer scale and also to determine if there is any homogeneity within the size distribution of the particles. The use of XRD will be vital in determining the crystallinity of the carbon core. Quantum yield tests will be used in conjunction with the XPS test to determine how efficient the CQDs are in absorbing photons. Lastly, X-ray photoelectron spectroscopy (XPS) will be another useful tool that can help elucidate the chemical bonding environment of the carbon, oxygen, and nitrogen atoms on the surface of the CQDs, which will provide more insights regarding the FTIR results.

Selectivity studies on a diverse set of metal ions need to be carried out before one can confidently claim any practical application of the Fe^{3+} detection using the material at hand. If the selectivity is not high enough for the CQDs, there are ways to solve such a problem – nitrogen doping, attaching chelating agents, etc., have been extensively used in the past for making CQDs selective. After completing selectivity tests, one will then need to conduct the sensing experiment in real water samples spiked with the analyte.

References

[1] Ananta Raj Devkota, DD Dhakal, DM Gautam, and JP Dutta. Assessment of fruit and vegetable losses at major wholesale markets in nepal. *International journal of applied sciences and biotechnology*, 2(4):559–562, 2014.

[2] Bed P Khatiwada, Shanta Karki, Purushottam P Khatiwada, and Kishor C Dahal. Postharvest and quality management of fruits and vegetables in nepal. In *Agriculture, Natural Resources and Food Security: Lessons from Nepal*, pages 69–82. Springer, 2022.

[3] Mohammed Abdullah Issa, Zurina Z. Abidin, Shafreeza Sobri, Suraya Rashid, Mohd Adzir Mahdi, Nor Azowa Ibrahim, and Musa Y. Pudza. Facile synthesis of nitrogen-doped carbon dots from lignocellulosic waste. *Nanomaterials*, 9(10):1500, 2019.

[4] Habtamu Fekadu Etefa, Aster Aberra Tessema, and Francis Birhanu Dejene. Carbon dots for future prospects: synthesis, characterizations and recent applications: a review (2019–2023). *C*, 10(3):60, 2024.

[5] Noona Parambil, Arish Dasan, Amrutha Premkumar, Renuka Neeroli, and Selwin Raphael. Blue luminescent carbon quantum dots derived from diverse banana peels for selective sensing of fe(iii) ions. *Sensors International*, 6:100301, 09 2024.

[6] Xiaoyou Xu, Robert Ray, Yunlong Gu, Harry J Ploehn, Latha Gearheart, Kyle Raker, and Walter A Scrivens. Electrophoretic analysis and purification of fluorescent single-walled carbon nanotube fragments. *Journal of the American Chemical Society*, 126(40):12736–12737, 2004.

[7] Ya-Ping Sun, Bing Zhou, Yi Lin, Wei Wang, KA Shiral Fernando, Pankaj Pathak, Mohammed Jaouad Meziani, Barbara A Harruff, Xin Wang, Haifang Wang, et al. Quantum-sized carbon dots for bright and colorful photoluminescence. *Journal of the American Chemical Society*, 128(24):7756–7757, 2006.

[8] Anirudh Sharma and Joydeep Das. Small molecules derived carbon dots: synthesis and applications in sensing, catalysis, imaging, and biomedicine. *Journal of nanobiotechnology*, 17(1):92, 2019.

[9] Chuang He, Peng Xu, Xuanhan Zhang, and Wujian Long. The synthetic strategies, photoluminescence mechanisms and promising applications of carbon dots: Current state and future perspective. *Carbon*, 186:91–127, 2022.

[10] Junjie Shang, Qian Zhou, Kehan Wang, and Yunlin Wei. Engineering of green carbon dots for biomedical and biotechnological applications. *Molecules*, 29(18):4508, 2024.

[11] Salah Elkun, Mohsen Ghali, Taher Sharshar, and Mohsen Mohamed Mosaad. Green synthesis of fluorescent n-doped carbon quantum dots from castor seeds and their applications in cell imaging and ph sensing. *Scientific Reports*, 14(1):27927, 2024.

[12] Raji Atchudan, Thomas Nesakumar Jebakumar Immanuel Edison, Mani Shanmugam, Suguna Perumal, Thirunavukkarasu Somanathan, and Yong Rok Lee. Sustainable synthesis of carbon quantum dots from banana peel waste using hydrothermal process for in vivo bioimaging. *Physica E: Low-dimensional Systems and Nanostructures*, 126:114417, 2021.

[13] Rawan H Alansari, Esraa M Bakhsh, Lenah R Altamimi, Kalsoom Akhtar, and Sher Bahadar Khan. One-step microwave-assisted fabrication of carbon dots as efficient fluorescent chemosensors for hg2+ and fe3+ detection. *Sensors*, 25(24):7452, 2025.

[14] Sihua Zeng, Chunrong Qin, Yuzhu Zhang, Haoyu Chen, and Hua Lin. A green-synthesized fluorescent carbon dot probe derived from banana peel for cellular imaging and sensing of tetracycline. *Materials*, 18(22):5211, 2025.

[15] Trong Nghia Nguyen, Phuoc Anh Le, and Viet Bac T Phung. Facile green synthesis of carbon quantum dots and biomass-derived activated carbon from banana peels: synthesis and investigation. *Biomass Conversion and Biorefinery*, 12(7):2407–2416, 2022.

[16] Klaudia Jomova, Suliman Y Alomar, Eugenie Nepovimova, Kamil Kuca, and Marian Valko. Heavy metals: toxicity and human health effects. *Archives of toxicology*, 99(1):153–209, 2025.

[17] Wen lin Zhong and Jin yan Yang. Fluorescent carbon quantum dots for heavy metal sensing. *Science of The Total Environment*, 957:177473, 2024.

[18] M Ghali, WS Mabior, H Soliman, M Sami, and MK Elnimr. Ultrasensitive optical detection of fe3+ ions using fluorescent carbon quantum dots derived from simmondsia chinensis jojoba leaves. *Scientific Reports*, 15(1):40375, 2025.

[19] Chetsada Phaenark, Yutthana Phankamolsil, and Weerachon Sawangproh. Ecological and health implications of heavy metal bioaccumulation in thai fauna: A systematic review. *Ecotoxicology and Environmental Safety*, 285:117086, 2024.

[20] Li Zhao, Yesheng Wang, Xihui Zhao, Yujia Deng, and Yanzhi Xia. Facile synthesis of nitrogen-doped carbon quantum dots with chitosan for fluorescent detection of fe3+. *Polymers*, 11(11):1731, 2019.

[21] Zhaochuan Yu, Chao Deng, Wenhui Ma, Yuqian Liu, Chao Liu, Tingwei Zhang, and Huining Xiao. Microwave-assisted synthesis of n, s co-doped carbon quantum dots for fluorescent sensing of fe (iii) and hydroquinone in water and cell imaging. *Nanomaterials*, 14(22):1827, 2024.

[22] Dianwei Zhang, Furui Zhang, Yonghong Liao, Fenghuan Wang, and Huilin Liu. Carbon quantum dots from pomelo peel as fluorescence probes for "turn-off–on" high-sensitivity detection of fe3+ and l-cysteine. *Molecules*, 27(13):4099, 2022.

[23] Manisha Kumari, Ganga Ram Chaudhary, Savita Chaudhary, Ahmad Umar, Sheikh Akbar, and Sotirios Baskoutas. Bio-derived fluorescent carbon dots: synthesis, properties and applications. *Molecules*, 27(16):5329, 2022.

[24] Adhimoorthy Prasannan and Toyoko Imae. One-pot synthesis of fluorescent carbon dots from orange waste peels. *Industrial & Engineering Chemistry Research*, 52(44):15673–15678, 2013.

[25] Wooseok Lee and Seonghyuk Ko. Synthesis and characterization of lignocellulose-based carbon quantum dots (cqds) and their antimicrobial and antioxidant functionalities. *Molecules*, 30(3):667, 2025.

[26] Yustinus Purwamargapratala, Anne Zulfia, Evvy Kartini, Syan Zamir Zidane, Sri Handayani, and Tegar Pratama Kayong Wardana. Synthesis and characterization of carbon quantum dots from banana peel (musa paradisiaca forma typica) as additive for lithium-ion battery. In *AIP Conference Proceedings*, volume 3213, page 070005. AIP Publishing LLC, 2024.

[27] Surendran Pandiyan, Lakshmanan Arumugam, Sakthy Priya Srirengan, Rameshkumar Pitchan, Pushpalatha Sevugan, Karthik Kannan, Geetha Pitchan, Tejaswi Ashok Hegde, and Vinitha Gandhirajan. Biocompatible carbon quantum dots derived from sugarcane industrial wastes for effective nonlinear optical behavior and antimicrobial activity applications. *ACS omega*, 5(47):30363–30372, 2020.

[28] Zubair MSH Khan, Raja Saifu Rahman, Shama Islam, M Zulfequar, et al. Hydrothermal treatment of red lentils for the synthesis of fluorescent carbon quantum dots and its application for sensing fe3+. *Optical Materials*, 91:386–395, 2019.

[29] Sheila N Baker and Gary A Baker. Luminescent carbon nanodots: emergent nanolights. *Angewandte Chemie International Edition*, 49(38):6726–6744, 2010.

[30] Shi Ying Lim, Wei Shen, and Zhiqiang Gao. Carbon quantum dots and their applications. *Chemical Society Reviews*, 44(1):362–381, 2015.

[31] Shoujun Zhu, Qingnan Meng, Lei Wang, Junhu Zhang, Yubin Song, Han Jin, Kai Zhang, Hongchen Sun, Haiyu Wang, and Bai Yang. Highly photoluminescent carbon dots for multicolor patterning, sensors, and bioimaging. *Angewandte Chemie International Edition*, 52(14), 2013.

[32] Swagatika Sahu, Birendra Behera, Tapas K Maiti, and Sasmita Mohapatra. Simple one-step synthesis of highly luminescent carbon dots from orange juice: application as excellent bio-imaging agents. *Chemical communications*, 48(70):8835–8837, 2012.

[33] Dengyu Pan, Jingchun Zhang, Zhen Li, and Minghong Wu. Hydrothermal route for cutting graphene sheets into blue-luminescent graphene quantum dots. *Advanced materials*, 22(6):734–738, 2010.

[34] Youfu Wang and Aiguo Hu. Carbon quantum dots: synthesis, properties and applications. *Journal of Materials Chemistry C*, 2(34):6921–6939, 2014.

[35] Yongqiang Dong, Jingwei Shao, Congqiang Chen, Hao Li, Ruixue Wang, Yuwu Chi, Xiaomei Lin, and Guonan Chen. Blue luminescent graphene quantum dots and graphene oxide prepared by tuning the carbonization degree of citric acid. *Carbon*, 50(12):4738–4743, 2012.

[36] Libin Tang, Rongbin Ji, Xueming Li, Gongxun Bai, Chao Ping Liu, Jianhua Hao, Jingyu Lin, Hongxing Jiang, Kar Seng Teng, Zhibin Yang, et al. Deep ultraviolet to near-infrared emission and photoresponse in layered n-doped graphene quantum dots. *ACS nano*, 8(6):6312–6320, 2014.

[37] Xian Wen Tan, Ain Nadirah Binti Romainor, Suk Fun Chin, and Sing Muk Ng. Carbon dots production via pyrolysis of sago waste as potential probe for metal ions sensing. *Journal of analytical and applied pyrolysis*, 105:157–165, 2014.

[38] Hui Peng and Jadranka Travas-Sejdic. Simple aqueous solution route to luminescent carbogenic dots from carbohydrates. *Chemistry of Materials*, 21(23):5563–5565, 2009.

[39] LI Cao, Mohammed J Meziani, Sushant Sahu, and Ya-Ping Sun. Photoluminescence properties of graphene versus other carbon nanomaterials. *Accounts of chemical research*, 46(1):171–180, 2013.

[40] Wen Shi, Xiaohua Li, and Huimin Ma. A tunable ratiometric ph sensor based on carbon nanodots for the quantitative measurement of the intracellular ph of whole cells. *Angewandte Chemie (International ed. in English)*, 51(26):6432–6435, 2012.

[41] Xinyun Zhai, Peng Zhang, Changjun Liu, Tao Bai, Wenchen Li, Liming Dai, and Wenguang Liu. Highly luminescent carbon nanodots by microwave-assisted pyrolysis. *Chemical communications*, 48(64):7955–7957, 2012.

[42] Jia Zhang and Shu-Hong Yu. Carbon dots: large-scale synthesis, sensing and bioimaging. *Materials Today*, 19(7):382–393, 2016.

[43] Li Zhou, Youhui Lin, Zhenzhen Huang, Jinsong Ren, and Xiaogang Qu. Carbon nanodots as fluorescence probes for rapid, sensitive, and label-free detection of hg 2+ and biothiols in complex matrices. *Chemical communications*, 48(8):1147–1149, 2012.

[44] Haipeng Liu, Tao Ye, and Chengde Mao. Fluorescent carbon nanoparticles derived from candle soot. *Angewandte chemie*, 119(34):6593–6595, 2007.

[45] Xin Ting Zheng, Arundithi Ananthanarayanan, Kathy Qian Luo, and Peng Chen. Glowing graphene quantum dots and carbon dots: properties, syntheses, and biological applications. *small*, 11(14):1620–1636, 2015.

[46] F. Yang et al. A true biomass standout: Preparation and application of biomass-derived carbon quantum dots. *BioResources*, 19(3), 2024.

[47] M. Kumar, S. Chinnathambi, N. Bakhori, N. Abu, F. Etezadi, V. Thangavel, et al. Biomass-derived carbon dots as fluorescent quantum probes to visualize and modulate inflammation. *Scientific Reports*, 14(1):12665, 2024.

[48] S. Ye, M. Zhang, J. Guo, J. Song, P. Zeng, J. Qu, et al. Facile synthesis of green fluorescent carbon dots and their application to fe3+ detection in aqueous solutions. *Nanomaterials*, 12(9):1487, 2022.

[49] Kullaiah Byrappa and Tadafumi Adschiri. Hydrothermal technology for nanotechnology. *Progress in crystal growth and characterization of materials*, 53(2):117–166, 2007.

[50] V. Magesh, A. K. Sundramoorthy, and D. Ganapathy. Recent advances on synthesis and potential applications of carbon quantum dots. *Frontiers in Materials*, 9:906838, 2022.

[51] X. Dong, H. Qi, Z. Zhai, W. Li, and P. Zhang. Probing the fluorescence quenching mechanism of n-doped carbon quantum dots by inorganic ions. *Microchemical Journal*, 197:109854, 2024.

[52] Runxia Wang, Xiufang Wang, and Yimin Sun. One-step synthesis of self-doped carbon dots with highly photoluminescence as multifunctional biosensors for detection of iron ions and ph. *Sensors and Actuators B: Chemical*, 241:73–79, 2017.

[53] X. Feng, Y. Xie, W. Zhao, M. Green, L. Liu, and X. Chen. Fluorescence quenching effects of fe3+ ions on carbon dots. *Spectroscopy*, 36(7):31–36, 2021.

[54] H. L. Yang, L. F. Bai, Z. R. Geng, H. Chen, L. T. Xu, Y. C. Xie, et al. Carbon quantum dots: Preparation, optical properties, and biomedical applications. *Materials Today Advances*, 18:100376, 2023.

[55] Mehedi Hasan, Balachandran Baheerathan, Shrikanta Sutradhar, Ronak Shahbandinejad, Sudip Rakshit, Janusz Kozinski, Dongbing Li, Yulin Hu, and Kang Kang. Microwave-assisted synthesis of biomass-derived n-doped carbon dots for metal ion sensing. *Carbon Research*, 4(1):49, 2025.